Journal of Medicinal and Chemical Sciences 6 (2023) 280-303

Journal of Medicinal and Chemical Sciences

Journal homepage: http://www.jmchemsci.com/

Original Article

Ligand Adducts of Bis(acetylacetonato) Copper(II), Bis(3-chloroacetylacetonato) Copper(II) with 4,4'-bipyridine, and Propylene Spacered Bis-viologen

Azhar H. Gatea[1,2,*], W. S. Abdul-Hassan[1], S. A. Ali[1], Z. M. Mahdi[3]

[1]*University of Thi-Qar, College of Science, Department of Chemistry, 64001 Nasiriya, Iraq*
[2]*University of Thi-Qar, Faculty of Veterinary, Branch of Physiology, Pharmaceutical and Biochemistry, 64007 Shatrah, Iraq*
[3]*Mazaya University College, Department of Pharmacy, 64001 Nasiriya, Iraq*

ARTICLE INFO

Article history

Receive: 2022-06-08
Received in revised: 2022-07-21
Accepted: 2022-08-25
Manuscript ID: JMCS-2208-1621
Checked for Plagiarism: **Yes**
Language Editor:
Dr. Fatimah Ramezani
Editor who approved publication:
Prof. Dr. Hassan Karimi-Maleh

DOI:10.26655/JMCHEMSCI.2023.2.10

KEYWORDS

Acetylacetone
Adduct
4,4`-Bipyridine
Viologen
π-Dimer
Copper (II) complexes

ABSTRACT

Bis(acetylacetonato) copper (II): CuA, bis(3-chloroacetylacetonato) copper: CuA-Cl, and their adducts with 4,4`-bipyridine are synthesized. These copper (II) complexes are characterized by mass, FT-IR, UV-Visible, and XRD spectrometries. The interaction of copper (II) complexes: CuA and CuA-Cl with 4,4`-bipyridine, Bpy, and bis-viologen, $V_2^{2+}.2PF_6^-$ are studied in solution by electronic absorption spectroscopy. The solutions of adducts happened between CuA and CuA-Cl with $V_2^{2+}.2PF_6^-$ are reduced by activated Zn powder to afford viologen-based switches within adducts structures.

GRAPHICAL ABSTRACT

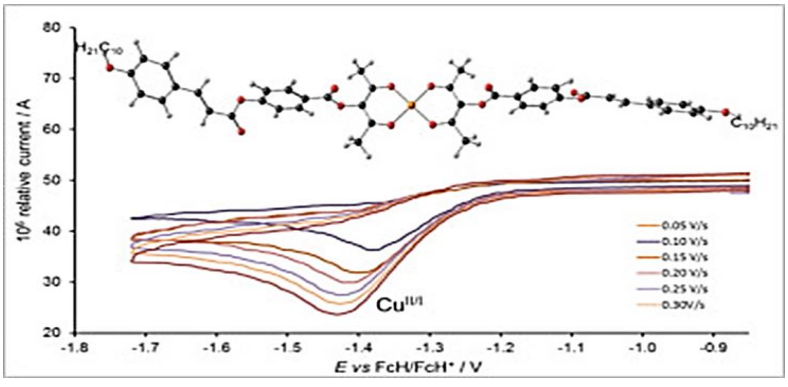

* Corresponding author: Azhar H. Gatea
✉ E-mail: Email: azharhameedgatea@gmail.com

Introduction

β-diketones have three reactive sites, the two carbonyl groups, and the central carbon atom with three substituents sites such as R_1, R_2, and R_3. They have been documented as ligands and extracting agents for numerous of metals [1–3] *β*-diketones act as neutral, monoanionic, and dianionic *β*-diketones ligand under appropriate conditions. Metal *β*-diketone showed complexes in four types I, II, III, and IV, as displayed in Scheme 1 [4].

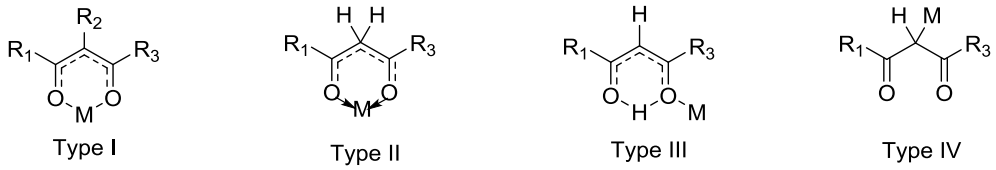

Scheme 1: Coordination modes of *β*-diketone [4]

X-ray crystallography discovered additional patterns of these types of complexes due to the development of X-rays apart from the common classical *O,O*-bidentate chelates [5]. *β*-diketones and their complexes are characterized and extensively studied by ^{1}H-NMR, ^{13}C-NMR, IR, UV-visible spectroscopies, X-ray diffraction, cyclic voltammetry, and thermal analysis techniques [6–9].

In fact, *β*-diketones exist in both tautomeric keto and enol forms. Tautomerization depends strongly on the substituents R_1, R_2, and R_3 as donating, or withdrawing groups, and depends also on temperature, concentration, solvent, and phase. The tautomeric keto form is more stable in polar solvents than the tautomeric enol form which is more stable in nonpolar solvents (Scheme 2) [10].

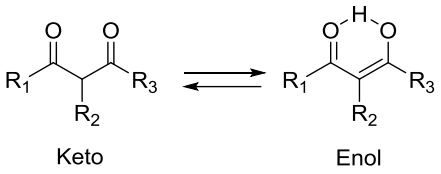

Scheme 2: Tautomerization of *β*-diketone [11]

The tautomerization was studied in a gas phase by Gas electron diffraction [11, 12], in the solution by IR and NMR techniques, and in the solid state by X-ray crystal diffraction [13].

Our objectives of this study were initially to synthesize and investigate properties of adducts complexes: CuABpy and CuA-ClBpy that were formed among the copper (II) complexes of acetylacetone and 3-chloroacetylacetone: CuA and CuA-Cl, respectively with 4,4`-Bipyridine. Likewise, this stdy aimed to follow the formation of these two adducts CuABpy and CuA-ClBpy in solution as well as the formation of the adducts $CuAV_2$ and $CuA\text{-}ClV_2$ occured with both copper (II) complexes with propylene spacered bis-viologen: $V_2^{2+}.2PF_6$. Next, the formation of redox-induced π-dimers of the coordinated bis-viologen moieties within the adducts: $CuAV_2$ and $CuA\text{-}ClV_2$ was aimed to be investigated.

Experimental

Chemical Reagents

Reagents and solvents were commercially sourced and used without further purification. 2,4-Pentanedione, 3-Chloro-2,4-pentanedione, 4,4`-Bipyridine, Iron(II)tetrafluoroborate hexahydrate, Zinc(II)tetrafluoroborate hydrate, Copper(II)tetrafluoroborate hexahydrate, and Anhydrous copper(II) acetate were from BHD. Methanol, Acetonitrile, and Dimethylformamide were from Chem-Lab/Belgium. Dichloromethane, Diethyl ether, Chloroform, Acetone, Hexane, and Benzene were from Romil/England. Absolute ethanol was from Haymankimia/ England and Ethyl acetate was from Scharlau/Eu.

Instrumentation

FT-IR spectra are recorded for solid samples discs by using CsI pellets over the spectral range from

150 to 4000 cm^{-1} by using SHIMADZU/FT-IR Affinity-1 spectrophotometer and the UV-visible absorption spectra over the spectral range from 200 to 900 nm are recorded on a T90+ UV-visible spectrometer (PG Instruments Ltd) by using conventional quartz cell having an optical path length of 1cm. The uncorrected melting points of the prepared viologen derivatives were measured by using melting point/SMP3 at Department of Chemistry, College of Science, University of Thi-Qar, Iraq. Mass spectra are recorded by using 5973 Network Mass Selective Detector manufactured by Agilent Technology (HP) with ion source of Electron Impact (EI) 70 ev in the Department of Chemistry, Tehran University, Iran. The thermogravimetric analysis of metal complexes were recorded on TGA-50, in Department of Chemistry, College of education for pure Science, University of Basra. The XRD measurements of complexes were carried out by using Panalytical diffractometer with Cu Kα radiation, Iran.

Syntheses of Cu(II) Complexes

Synthesis of bis(acetylacetonato) copper (II), CuA [7]

A solution of acetyl acetone (1 mL, 9.730 mmol, 2 eq) dissolved in 2 ml of methanol was added gradually during 15 minutes with stirring into a solution of copper acetate (0.884 g, 4.865 mmol, 1 eq) dissolved in 36 ml of methanol-water mixture (1:1). The mixture was refluxed for 2 hours with stirring. The resulting precipitate was collected by filtration, washed with water, methanol, and then dried under vacuum to afford the complex CuA as blue solid, yield (1.2 g, 95%), m.p.: 230 °C. It is soluble in acetonitrile, chloroform, and DMF. It is not soluble in water, methanol, ethanol, ethyl acetate, acetone, diethyl ether, benzene, and hexane (Scheme 3, Table 1).

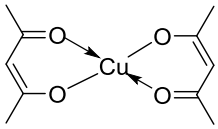

Scheme 3: bis(acetylacetonato) copper (II), CuA

Synthesis of bis(3-chloroacetylacetonato) copper, CuA-Cl [7]

A solution of 3-chloro-acetyl acetone (1 ml, 8.850 mmol, 2 eq) dissolved in 2 ml of methanol was added gradually during 15 minutes with stirring into a solution of copper acetate (0.804 g, 4.426 mmol, 1 eq) dissolved in 36 ml of methanol-water mixture (1:1). The mixture was refluxed for 2 hours with stirring. The resulting precipitate was collected by filtration, washed with water, methanol, and then dried under vacuum to afford the complex CuA-Cl as greenish-grey solid, yield (1.4 g, 97%), m.p.: 273 °C. It is soluble in acetonitrile, chloroform, methanol, ethanol, ethyl acetate, acetone, DCM, and DMF. It is not soluble in water, diethyl ether, benzene, and hexane (Scheme 4).

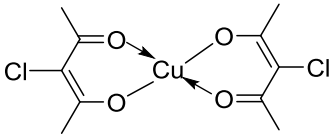

Scheme 4: bis(3-chloroacetylacetonato) copper, CuA-Cl

Synthesis of CuApy complex [14]

4,4`-Bipyridine (0.59 g, 3.82 mmol, 10 eq) dissolved in minimum amount of acetonitrile was added with 24 hours stirring into a solution of CuA complex (0.1 g, 0.382 mmol, 1 eq) dissolved in minimum amount of acetonitrile. The resulting precipitate was collected by filtration, washed with acetonitrile, and then dried under vacuum to afford CuApy as cyan solid, yield (0.15 g, 94%), m.p.: 195°C. It is soluble in DMF. It is not soluble in water, methanol, ethanol, ether, hexane, benzene, acetonitrile, chloroform, acetone, and ethyl acetate (Scheme 5).

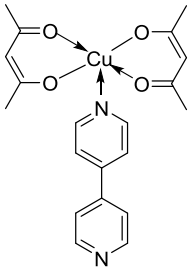

Scheme 5: CuApy complex

Table 1: Physical properties of complexes

Compound	Color	M.wt (g/mol)	M.p (°C)
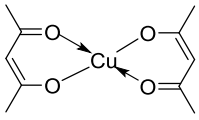 CuA	Blue 	261.76	230
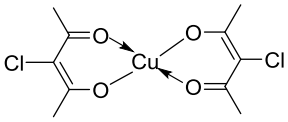 CuA-Cl	Greenish-grey 	330.65	273
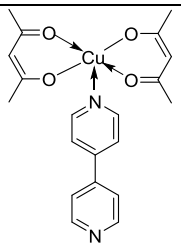 CuABpy	Cyan 	417.95	195
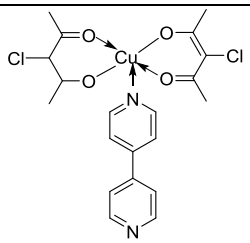 CuA-ClBpy	Green 	486.84	191

Syntheses of Cu(II)Complexes

Four complexes are synthesized as follows:

Syntheses of bis(acetylacetonato) copper (II), CuA, and bis(3-chloroacetylacetonato) copper, CuA-Cl complexes

The syntheses of each CuA and CuA-Cl are done in one step that involves complexion reaction between 2 equivalents of acetyl acetone or 3-chloro-acetyl acetone with 1 equivalent of copper acetate to afford CuA as a blue solid in yield 95% or CuA-Cl as a greenish-grey solid in yield 97% (Scheme 6).

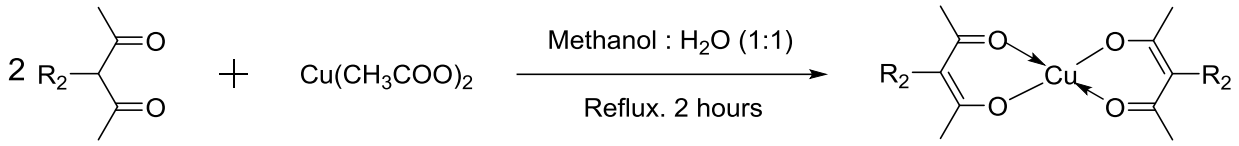

R_2= H: acetylacetone or
Cl: 3-chloro acetylacetone

R_2= H: CuA or Cl: CuA-Cl

Scheme 6: Syntheses of CuA and CuA-Cl

Syntheses of CuABpy and CuA-ClBpy complexes

The syntheses of CuABpy and CuA-ClBpy are done in one step that involves a reaction of big amount (10 equivalents) of 4,4`-Bipyridine with CuA or CuA-Cl complexes to afford CuABpy as a cyan solid in yield 94% or CuA-Clpy as a green solid in yield 95% (Scheme 7).

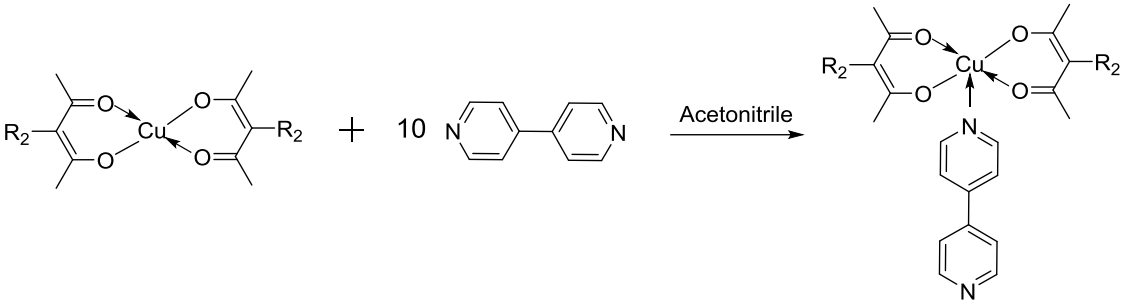

R_2= H: CuA or Cl: CuA-Cl

R_2= H: CuABpy or Cl: CuA-ClBpy

Scheme 7: Syntheses of CuABpy and CuA-ClBpy

Results and Discussion

Mass spectra of copper (II) complexes and their adducts

The electron impact mass spectra of complexes: CuA, CuA-Cl, and their adducts: CuABpy and CuA-ClBpy were recorded and showed peaks occurred at m/z= 261, 331, 417, and 487, respectively which were due to their molecular ions. These complexes structures were more confirmed by the appearance of other important peaks at m/z= 247, 293, 261, and 368 which were attributed to loss of one methyl group, chlorine atom, one bipyridine moiety, and both chlorine atom and methyl group, respectively [15].

FT-IR spectroscopy of copper (II) complexes and their adducts

FT-IR spectra of the complexes: CuA, CuA-Cl, and their adducts: CuABpy and CuA-ClBpy are recorded and displayed in Figure 1 (Table 2).

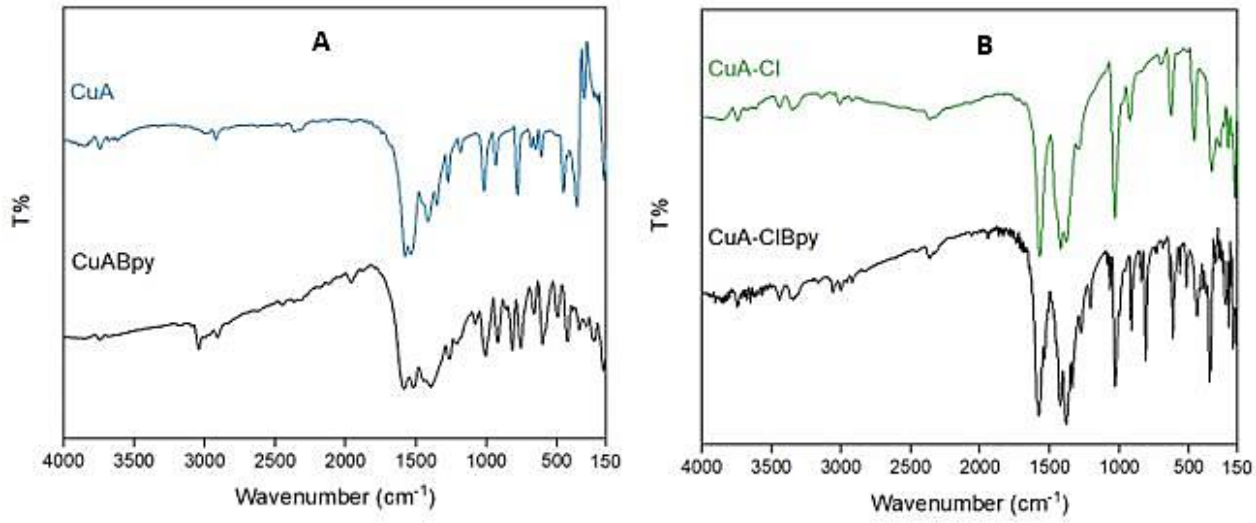

Figure 1: FT-IR spectra of (A) CuA and CuABpy, (B) CuA-Cl and CuA-ClBpy

Table 2: Important infrared data of copper (II) complexes

CuA **υ, cm^{-1}**	CuABpy υ, cm^{-1}	CuA-Cl υ, cm^{-1}	CuA-ClBpy υ, cm^{-1}	Assignment
----	**----**	3441, 3348	3444, 3336	υO-H of H_2O
3001	3039	3008	3055, 3001	υC-H of both aromatic and C=C-H
2920	2908	2920	2920	Aliphatic υC-H
1577, 1539	1585, 1519	1573	1577, 1539	υ C=C coupled with υ C=C + υC=N
1415, 1354	1410, 1396	1423, 1381	1423, 1381, 1338	Aliphatic C-H bending
1207, 1184	1265, 1207	1292	1280, 1207	υC-O
----	1080	----	1068	υC-N
1018	1006	1033	1033	Out-of-plane rocking of CH_3
933	918, 817	925, 806	914, 844, 810	Bending C-H of aromatic + υC-Cl
779	756	**----**	**----**	Bending C-H of olefinic
682, 651, 609	663, 601	628	617	υCu-O
----	586, 497	**----**	567, 520	υCu-N
455	428	462	439	Ring deformation

Both CuA-Cl and its adducts show two bands at 3441 cm^{-1} and 3348 cm^{-1} for CuA-Cl as well as 3444 cm^{-1} and 3336 cm^{-1} for CuA-ClBpy could be attributed to υO-H of H_2O [16]. The bands at 3001 cm^{-1} of CuA, 3039 cm^{-1} of CuABpy, 3008 cm^{-1} of CuA-Cl, and 3055 cm^{-1} and 3001 of CuA-ClBpy, these bands are attributed to stretching vibrations of both aromatic and C=C-H groups which confirm the coordination with bipyridine moiety. The metal complexes indicated bands at 2920 cm^{-1} of CuA, 2908 cm^{-1} of CuABpy, 2920 cm^{-1} of CuA-Cl, and 2920 cm^{-1} of CuA-ClBpy that are attributed to aliphatic C-H stretching vibrations [17].

The bands at 1577 cm^{-1}, 1539 cm^{-1} of CuA, 1585 cm^{-1} and 1519 cm^{-1} of CuABpy, 1573 cm^{-1} of CuA-Cl, and 1577 cm^{-1} and 1539 cm^{-1} of CuA-ClBpy are assigned to the stretching of C=C coupled with the stretching of both C=O and C=N groups in coordinated bipyridine moiety. The C-H bending vibrations occurred at 1415 cm^{-1} and 1354 cm^{-1} for CuA, 1410 cm^{-1} and 1396 cm^{-1} for CuABpy, 1423 cm^{-1} and 1381 cm^{-1} for CuA-Cl, 1423 cm^{-1}, and 1381 cm^{-1} and 1338 cm^{-1} for CuA-ClBpy. The bands at 1207 cm^{-1} and 1184 cm^{-1} of CuA, 1265 cm^{-1}, 1207 cm^{-1} of CuABpy, 1292 cm^{-1} of CuA-Cl, and 1280 cm^{-1} and 1207 cm^{-1} of CuA-ClBpy are assigned to the C-O bending coupled to stretching vibrations in C-CO-C group.

For adducts compounds: CuABpy and CuA-ClBpy, the bands at 1080 cm^{-1} and 1068 cm^{-1} were observed, respectively, these bands which are absent in their precursor complexes, are attributed to C-N bending vibrations which is another evidence to the coordination with bipyridine moiety. The FT-IR spectra showed out of plane bending vibrations of CH_3 groups at 1018 cm^{-1}, 1006 cm^{-1}, 1033 cm^{-1}, and 1033 cm^{-1} of CuA, CuABpy, CuA-Cl, and CuA-ClBpy, respectively.

The bands happened at 808-933 cm^{-1} included out of a plane bending of aromatic C-H and stretching of C-Cl. The bands at 779 cm^{-1} of CuA and 756 cm^{-1} of CuABpy are for out of plane bending vibrations of olefinic C=C-H groups. CuA showed bands at 682 cm^{-1}, 651 cm^{-1} and 609 cm^{-1}, CuABpy at 663 cm^{-1}, 601 cm^{-1}, CuA-Cl at 628 cm^{-1}, and CuA-ClBpy at 617 cm^{-1} which are assigned as υCu-O. Adducts showed bands of CuABpy at 586 cm^{-1} and 497 cm^{-1} and of CuA-ClBpy at 567 cm^{-1} and 520 cm^{-1} which could be attributed to υCu-N. whereas, the bands at 455 cm^{-1}, 428 cm^{-1}, 462 cm^{-1}, and 439 cm^{-1} of CuA, CuABpy, CuA-Cl, and CuA-ClBpy are attributed to the ring deformation, respectively [18, 19].

X-ray diffraction of the complexes

The XRD pattern of the complexes: CuA, CuA-Cl, and their adducts: CuABpy and CuA-ClBpy are recorded and depicted in Figure 2.

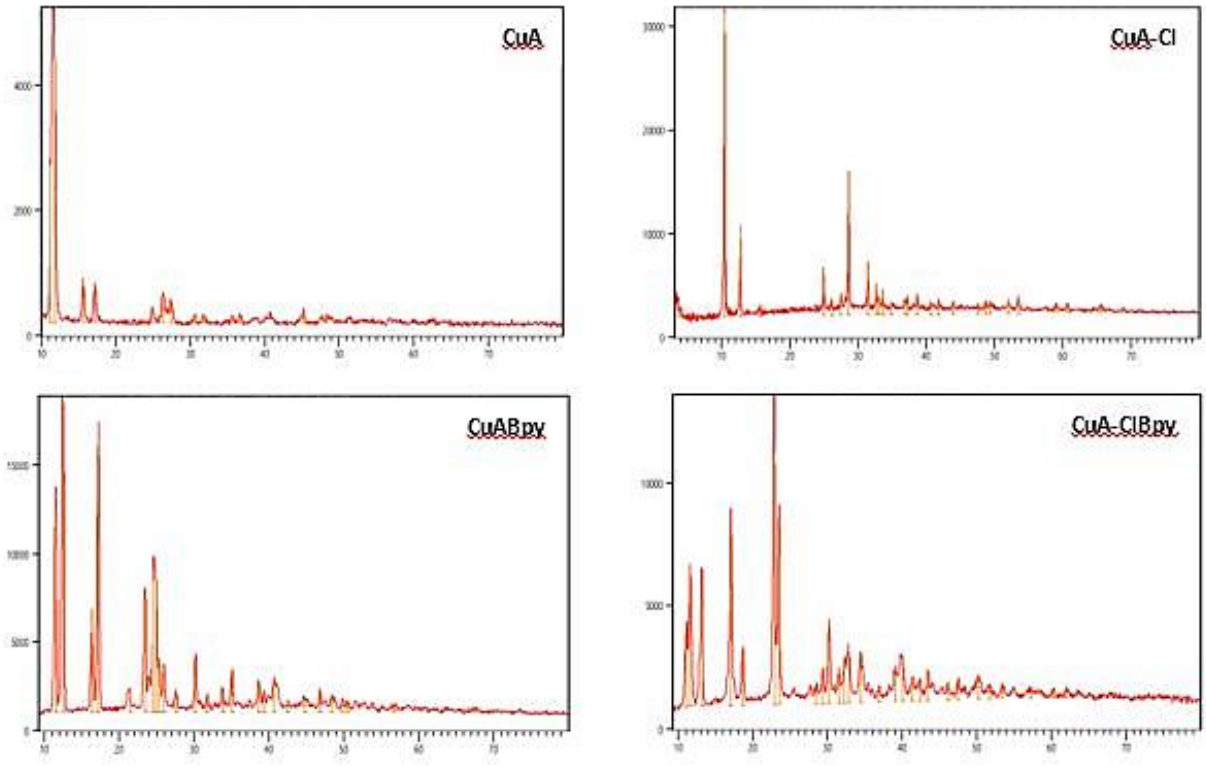

Figure 2: The XRD pattern of the CuA, CuA-Cl, CuABpy, and CuA-ClBpy complexes

The XRD patterns are shown at angles $10^0 < 2\theta < 80^0$. The largest peaks are observed at around 11.84^0, 10.44^0, 17.16^0, and 22.89^0 for CuA, CuA-Cl, CuABpy, and CuA-ClBpy. The crystallite size D and the strain ε are calculated from both Scherrer method and Williamson-Hall methods. Scherrer equation is widely used to estimate the crystallite size D from the measured diffraction peak profile. Scherrer equation submitted in Equation 1.

$$D = \frac{K\lambda}{\beta} \cdot \frac{1}{cos\theta} \quad (1)$$

Where, D represents the crystallite size, K is the shape factor (Scherrer constant equal to 0.94), λ is the wavelength of radiation in nanometer (λ equal to 0.15405 nm for Cu), β is full width at half maximum FWHM of the peak in radians, and θ is the diffraction angle of the peak [20, 21]. The Scherrer equation will be less reliable if a full width at half maximum FWHM caused by the instrumental broadening is bigger than that caused by the physical broadening [22]. The average model in Scherrer Equation included calculating crystallite sizes and averaging them. Table 3 contains the data for calculating the average crystallite sizes based on the Scherrer equation [23].

The Scherrer equation is the simple model which takes into account only the physical broadening and removes the instrumental broadening. Whereas, the Williamson-Hall model overcomes this problem [24].

$$\beta \cos\theta = \frac{K\lambda}{D} + 4\varepsilon \, sin\theta \quad (2)$$

According to Equation 2, plot of β cosθ (Y-axis) vs. 4 sinθ (X-axis) can be a linear relationship with a slope equal to the strain (ε) and the intercept is Kλ/D [25,26] See Figure 3.

Table 3: Values of crystallite size D calculated from average model in Scherrer Equation

$\frac{K\lambda}{\beta.\cos\theta}$ of CuA	$\frac{K\lambda}{\beta.\cos\theta}$ of CuA − Cl	$\frac{K\lambda}{\beta.\cos\theta}$ of CuABpy	$\frac{K\lambda}{\beta.\cos\theta}$ of CuA − ClBpy
41.01391863	104.649722	18.23257467	41.00416969
14.9231493	78.57186385	20.5303835	32.82044877
18.31065166	62.90185791	41.23366631	27.39123286
27.52153559	52.54823063	23.58651957	27.51223619
20.89774205	52.65398275	27.69472737	27.57234335
20.96192061	79.25392505	23.82143172	27.76070715
21.00723202	45.93197396	27.84337244	27.79269228
21.15223862	80.61279625	55.70304702	21.05187269
14.14665191	53.86815736	55.77480995	42.18721661
21.50189739	46.28274445	23.93162333	33.8127533
22.10485227	46.58562312	28.01985742	42.40770217
29.81544921	54.52488075	28.17674002	33.98937782
----	54.58175452	33.93934352	28.36706286
----	65.59558694	24.37517463	28.48662867
----	54.85065834	28.53290045	21.5104507
----	55.15127325	28.82967968	28.87052277
----	55.2152876	28.88754901	17.3748177
----	47.53362944	21.76088956	21.81607223
----	41.85519501	29.19762841	29.18011429
----	42.01203996	14.71727681	43.93697226
----	33.85874535	29.64745553	29.5723419
----	42.88442111	22.37577562	22.2909518
----	43.08217536	29.99808102	15.02507787
----	57.59138021	22.56867422	15.12142969
----	58.22580178	11.5909374	18.2780284
----	39.06960615	12.28055233	5.812241174
----	30.06637457	----	23.5927505
----	30.32424565	----	19.0321134
----	23.34572698	----	----
----	15.86066874	----	----
averages			
22.77976994	**51.64967763**	**27.43271813**	**34.0857923**

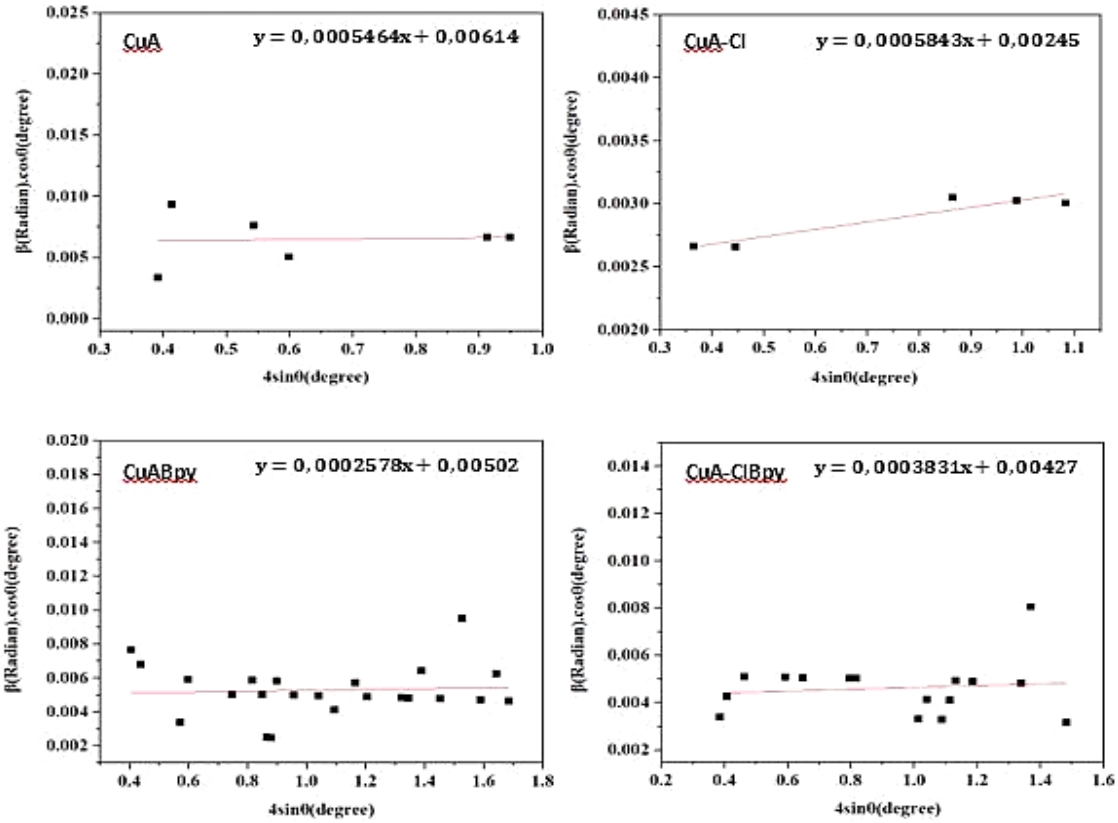

Figure 3: The UDM plot of the complexes: CuA, CuA-Cl, and their adducts: CuABpy and CuA-ClBpy

Table 4: Values of crystallite sizes and strain according to Williamson-Hall model

CuA		CuA-Cl		CuABpy		CuA-ClBpy	
D/nm	ε	ε	D/nm	D/nm	ε	D/nm	ε
22.83	5.464 x10^{-4}	5.843 x10^{-4}	57.21	27.92	3.831 x10^{-4}	32.83	2.578 x10^{-4}

The crystallite sizes were obtained from the UDM plots are 22.83, 57.21, 27.92, and 32.83 nm for CuA, CuA-Cl, CuABpy, and CuA-ClBpy, respectively. The values of crystalline sizes calculated from both methods are comparable and these values of the chlorinated complexes CuA-Cl and its adducts, CuA-ClBpy, are bigger than those of analogues CuA and its adducts CuABpy, respectively. Strain values were similar and occurred at 5.464x10^{-4}, 5.843x10^{-4}, 3.831x10^{-4}, and 2.578x10^{-4} for CuA, CuA-Cl, CuABpy, and CuA-ClBpy, respectively [21, 22, 25].

UV-Visible spectrometry of copper (II) complexes

Figure 4 represents electronic absorption spectra of CuA and CuA-Cl along with that of Cu(II) acetate in acetonitrile.

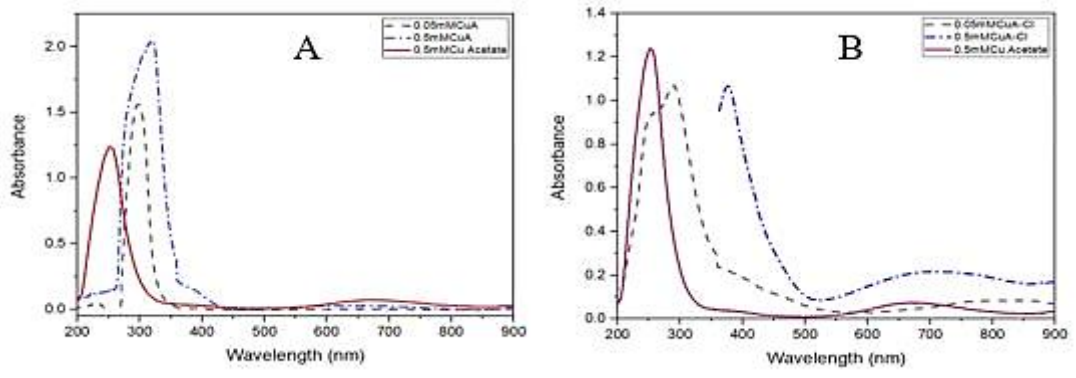

Figure 4: UV-visible spectra of (A) CuA complex, and Copper(II) acetate, (B) CuA-Cl complex, and Copper(II) acetate in acetonitrile at r.t by using quartz cell with path length of 1 cm

The d-d transition bands of CuA, CuA-Cl, and Cu(II) acetate occurred at 670 nm ($^2B_1g \rightarrow {}^2A_1g$), 700 nm ($^2B_1g \rightarrow {}^2A_1g$), and 648nm ($^2Eg \rightarrow {}^2T_2g$), respectively.[27]. The d-d transition bands of CuA and CuA-Cl are shifted to longer wavelengths by 22 nm and 52 nm, respectively compared with that of Cu(II) acetate which reflects that complexation happened and the ligand acetylacetone (2,4-Pentanedione) is stronger than the ligand 3-chloroacetylacetone (3-chloropentane-2,4-dione) [28].

The absorption spectra of the complexes are recorded in different solvents at two concentrations: low at 0.05 mM and high at 0.5 mM. These spectra of low and high concentrations showed clearly the UV and visible absorption bands, respectively. The electronic absorption data are listed in Table 3, and also see Figures 5-7. The visible absorption spectra of CuA showed two bands at 536 nm ($^2B_1g \rightarrow {}^2B_2g$), and 658 nm ($^2B_1g \rightarrow {}^2A_1g$) in chloroform; one band at 658 nm ($^2B_1g \rightarrow {}^2A_1g$) in acetonitrile and one band at 631 nm ($^2B_1g \rightarrow {}^2A_1g$) in DMF. These bands are attributed to the transitions within d-orbitals of copper ion of the CuA complex which indicates a square planar geometry[27].

The d-d transitions of CuA-Cl are noted at 409 nm ($^2B_1g \rightarrow {}^2Eg$), 531 nm ($^2B_1g \rightarrow {}^2B_2g$), and 668 nm ($^2B_1g \rightarrow {}^2A_1g$) in benzene; 423 nm ($^2B_1g \rightarrow {}^2Eg$) and 682 nm ($^2B_1g \rightarrow {}^2A_1g$) in chloroform; 410 nm ($^2B_1g \rightarrow {}^2Eg$), 538 nm ($^2B_1g \rightarrow {}^2B_2g$), 420 nm ($^2B_1g \rightarrow {}^2Eg$), and 616 nm ($^2B_1g \rightarrow {}^2A_1g$) in DCM; 409 nm ($^2B_1g \rightarrow {}^2Eg$) and 657 nm ($^2B_1g \rightarrow {}^2A_1g$) in ethyl acetate; 700 nm ($^2B_1g \rightarrow {}^2A_1g$) in acetonitrile; 414 nm ($^2B_1g \rightarrow {}^2Eg$) and 636 nm ($^2B_1g \rightarrow {}^2A_1g$) in ethanol; 417 nm ($^2B_1g \rightarrow {}^2Eg$) and 658 nm ($^2B_1g \rightarrow {}^2A_1g$) in DMF which indicate a square planar geometry. The transitions ($^2B_1g \rightarrow {}^2A_1g$), ($^2B_1g \rightarrow {}^2B_2g$), and ($^2B_1g \rightarrow {}^2Eg$) are very close in energy and appear as a single broad band [29].

The d-d transitions of CuA-Cl are shifted to a longer wavelength compared with those of CuA. The shifting was 24 nm in chloroform, 30 nm in acetonitrile, and 27 nm in DMF. Thus, shifts are another evidence that the ligand acetylacetone (2,4-Pentanedione) is stronger than the ligand 3-chloroacetylacetone (3-chloropentane-2,4-dione) [28].

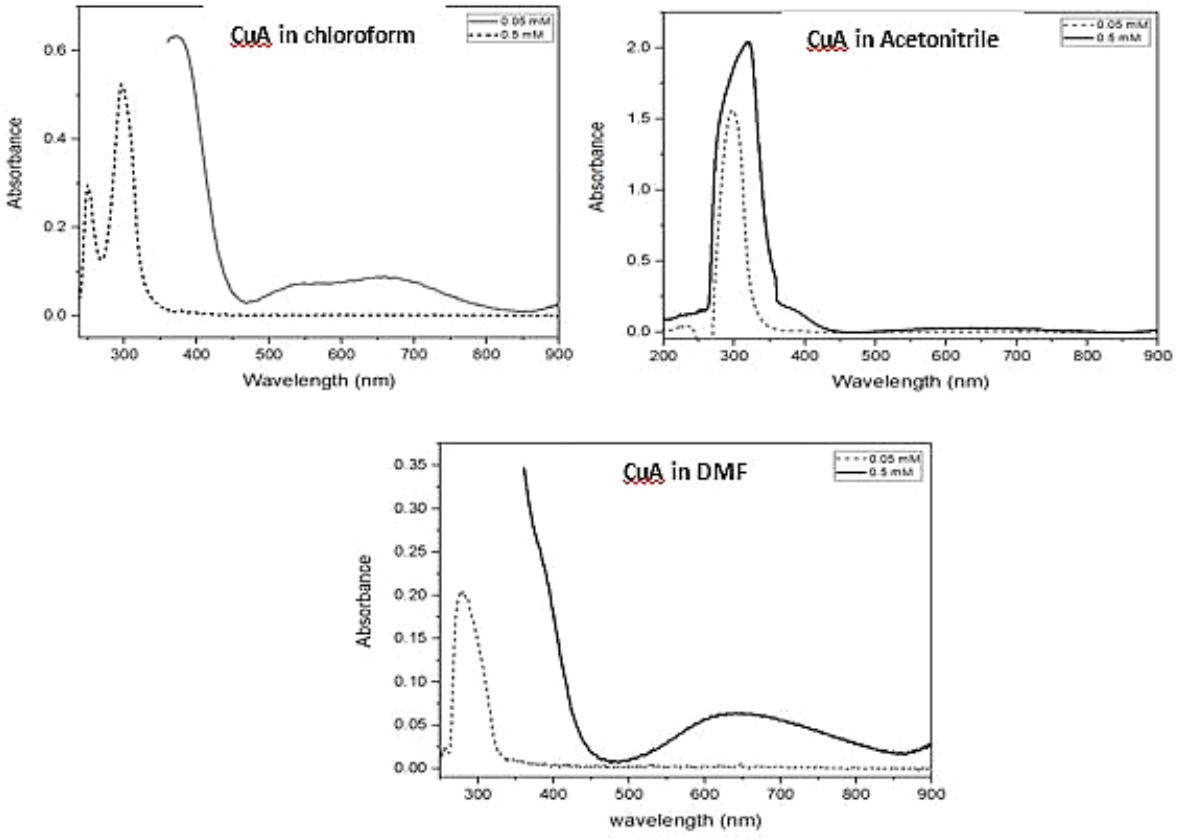

Figure 5: UV-visible spectra of 0.5 mM (solid line) and 0.05 mM (dotted line) of CuA complex in different solvent at r.t by using quartz cell with path length of 1 cm

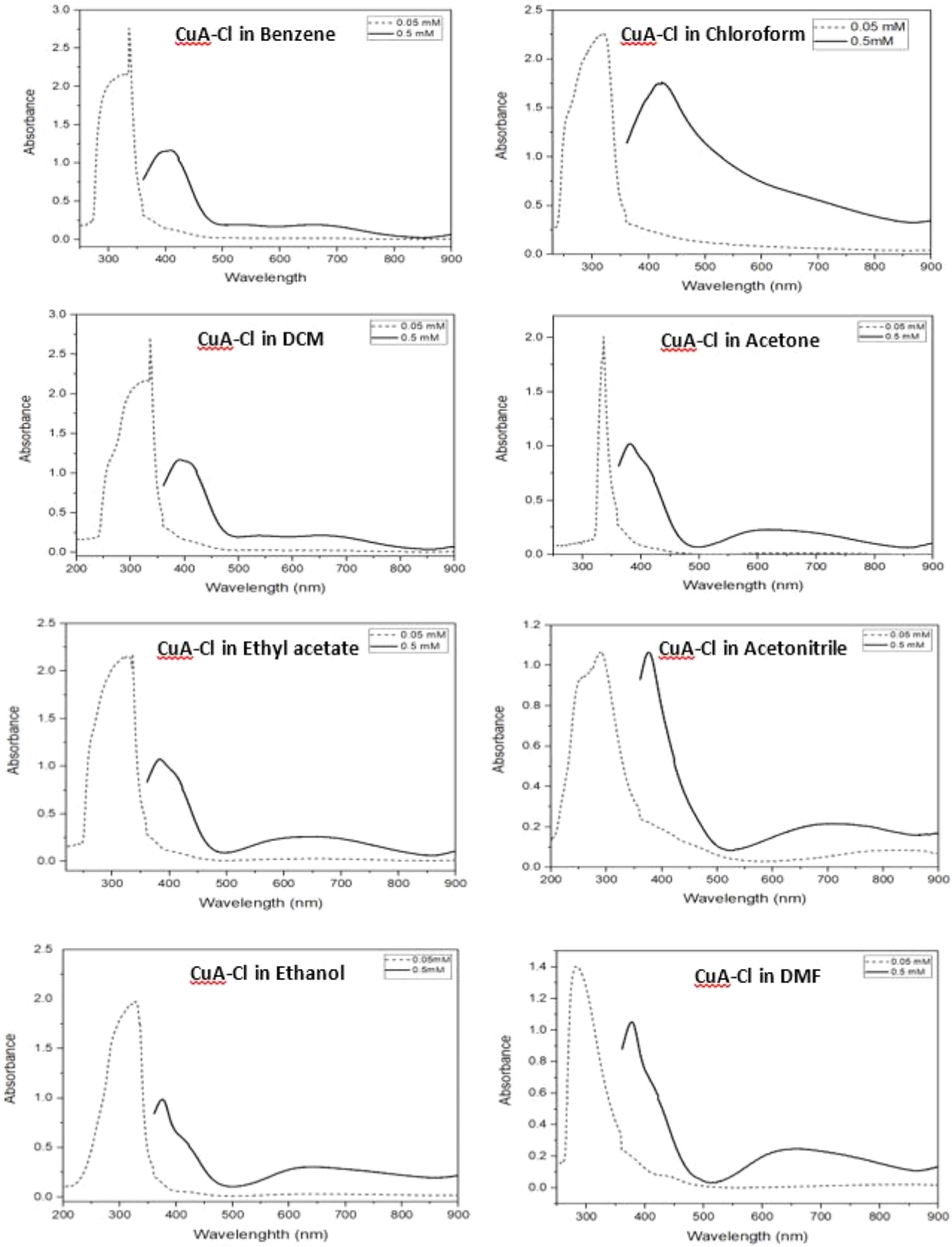

Figure 6: UV-visible spectra of 0.5 mM (solid line) and 0.05 mM (dotted line) of CuA-Cl complex in different solvent at r.t by using quartz cell with path length of 1 cm

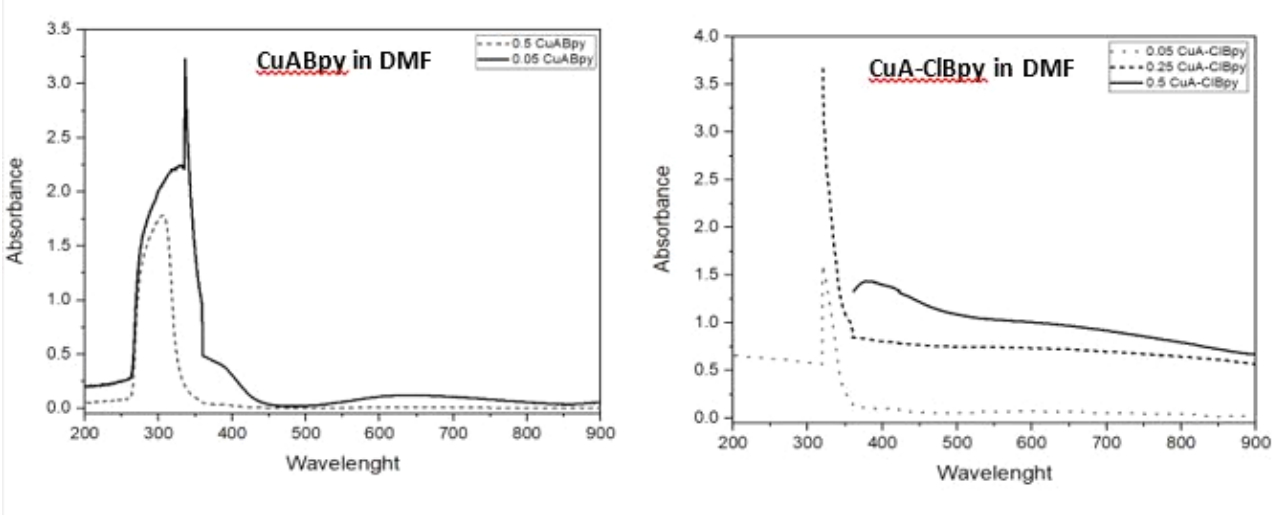

Figure 7: UV-visible spectra of 0.5 mM (solid line) and 0.05 mM (dotted line) of CuABpy and CuA-ClBpy complex in DMF at r.t by using quartz cell with path length of 1 cm

The ligand transitions of CuA complex are noted at 250 nm, 296 nm, and 370 nm in chloroform; 300 nm, 319 nm, and 381 nm in acetonitrile; 278 nm and 361 nm in DMF attributed to the coincidence between $n\rightarrow\pi^*$ and $\pi\rightarrow\pi^*$ electronic transitions which were attributed to the margin of both the $n\rightarrow\pi^*$ and $\pi\rightarrow\pi^*$ electronic transitions [30]. As for CuA-Cl complex occurred at 336 nm and 393 nm in benzene; 251 nm and 319 nm in chloroform; 256 nm, 306 nm, and 336 nm in DCM; 336 nm, and 381 nm in acetone; 336 nm and 384 nm in ethyl acetate; 251 nm, 291 nm, 377 nm, and 396 nm in acetonitrile; 327 nm and 375 nm in ethanol; 285 nm and 377 nm in DMF. Due to insolubility, the electronic absorption spectra of the adducts CuABpy and CuA-ClBpy are only recorded in DMF. The visible absorption transitions of CuABpy and CuA-ClBpy are observed at 644 nm ($^2B_1\rightarrow{}^2E$) and 635 nm ($^2B_1\rightarrow{}^2E$), respectively which are collected with a square pyramidal geometry [31,32]. The ligand transitions of adducts occurred at 307 nm, 313 nm, and 336 nm for CuABpy complex and at 321 nm and 379 nm for CuA-ClBpy complex which are attributed to $\pi\rightarrow\pi^*$ electronic transitions [33, 34] (Table 5).

Table 5: The electronic absorption data of complexes

Complex	Solvent	λ_{max}/nm ($\varepsilon/M^{-1}.cm^{-1}$)
CuA-Cl	Benzene	304(41380), 336 (55200), 393 (2320), 409 (2330), 531 (390), 668 (380)
CuA	Chloroform	250 (5920), 296 (10500), 370 (1260), 536 (140), 658 (170)
CuA-Cl	Chloroform	251 (28140), 319 (45280), 423 (3520), 682 (1170)
CuA-Cl	DCM	256 (20960), 306 (41560), 336 (54220), 391 (2330), 410 (2260), 538 (420), 655 (430)
CuA-Cl	Acetone	336 (40120), 381 (2040), 408 (1670), 616 (460)
CuA-Cl	Ethyl acetate	265(25480), 336 (43680), 384 (2150), 409 (1850), 657 (520)
CuA	Acetonitrile	300 (30920), 319 (4080), 381 (330), 670 (50)
CuA-Cl	Acetonitrile	251 (18540), 291 (21400), 377 (2130), 396 (3900), 700 (430)
CuA-Cl	Ethanol	327 (39460), 375 (1970), 414 (1150), 636 (600)
CuA	DMF	278 (4080), 361 (694), 631 (126)
CuA-Cl	DMF	285 (28020), 357(7160), 377 (2100), 417 (1250), 658 (496)
CuABpy	DMF	307 (35560), 313 (4320), 336 (6450), 358(1990), 388 (770), 644 (240)
CuA-ClBpy	DMF	321 (31580), 379 (2870), 635 (1960)

Interaction of copper complexes with ligands (formation of adducts)

Interaction of CuA and CuA-Cl as acceptors and 4,4`-bipyridine, Bpy as donor

The interaction between the acceptor: CuA, CuA-Cl, and the donor, Bpy was studied in solution by the UV-Visible spectroscopy. The resulted adduct: CuABpy and CuA-ClBpy were attained by mixing 1 and 2 equivalents of 4,4`-bipyridine with low and high concentrations of CuA and CuA-Cl complexes in DMF media.

The UV-Visible spectra of both CuA complex (black line) and its mixture with 1eq (blue line) and 2eq (red line) of 4,4`-bipyridine, Bpy are recorded in DMF media at two concentrations of CuA: low at 0.05 mM and high at 0.5 mM, as demonstrated in Figures 8 (A and B) and 11 (A and B), respectively. The electronic absorption data are listed in Table 4.

At low concentrations of CuA and Bpy mixtures, the d-d transitions of CuA occurred at 620 nm and 883 nm are shifted to 619 nm, 882 nm (blue shifts) as well as 631 nm and 896 nm (red shifts) for CuA mixtures with 1 eq and 2 eq Bpy, respectively. It seems that the differences in the d-d transitions noted for CuA and 2 eq of Bpy are more obvious than those of CuA and 1 eq Bpy compared with d-d transitions of free CuA. The bigger differences in d-d transitions could be correlated to the bigger interaction happened between Cu (II) ion and Bpy to afford the adduct compound CuABpy at the 2 eq Bpy, as illustrated in Table 4 and Figure 8.

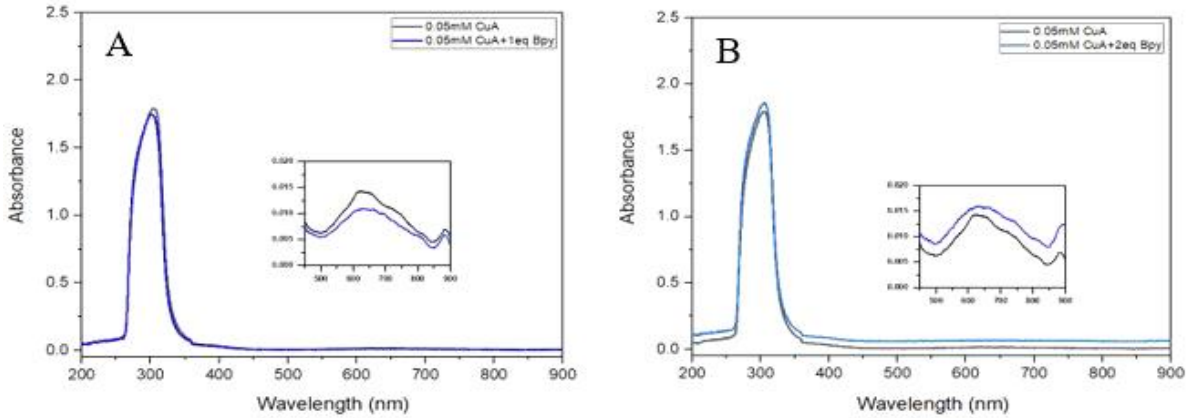

Figure 8: UV-Visible absorption spectra of 0.05 mM CuA (black lines in A and B), mixture of 0.05 mM CuA with 1eq Bpy (blue line in A), and mixture of 0.05 mM CuA with 2eq Bpy (blue line in B) in DMF at r.t by using quartz cell with path length of 1 cm

At high concentrations of CuA and Bpy mixtures, the d-d transitions of CuA occurred at 671 nm is shifted to 638 nm (blue shift) and 640 nm (blue shift) for CuA mixtures with 1 eq and 2 eq Bpy, respectively. It seems that the differences in the d-d transitions noted for mixture of CuA and 2 eq of Bpy are as same as those of mixture of CuA and 1 eq Bpy compared with d-d transitions of free CuA. These differences in d-d transitions could be due to the complexation of Cu (II) ion to Bpy moiety to afford the adduct compound CuABpy, as indicated in Table 4 and Figure 9.

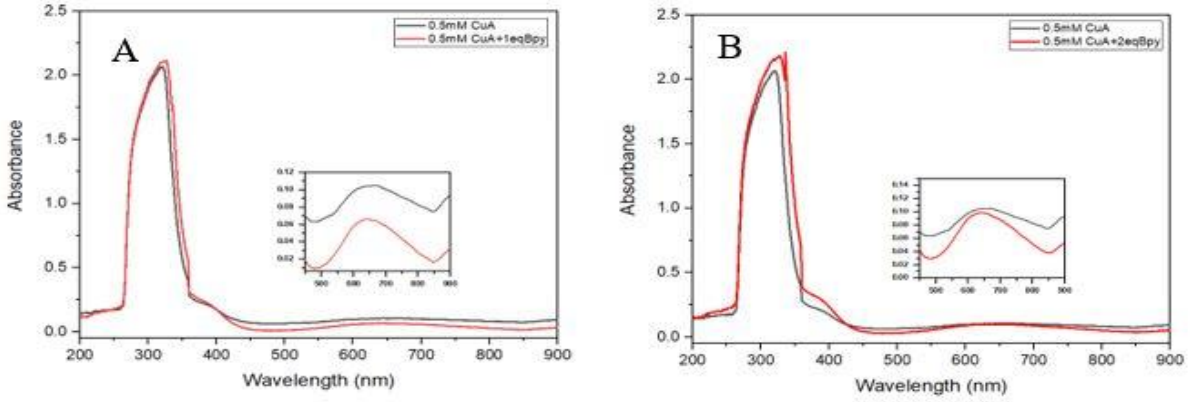

Figure 9: UV-Visible absorption spectra of 0.5 mM CuA (black lines in A and B), mixture of 0.5 mM CuA with 1eq Bpy (red line in A), and mixture of 0.5 mM CuA with 2eq Bpy (red line in B) in DMF at r.t by using quartz cell with path length of 1 cm

The complex, CuA is dissolved in the minimum amount of acetonitrile and mixed with big amount of 4,4`-bipyridine which is 10 eq. It was obtained directly the adduct, CuABpy as Cyan precipitate, as described in the item 3.3.1. and 3.4.1.1. It was noted that the solubility and the color of the adduct were very different from that of the precursor, CuA complex. The UV-visible absorption spectra are recorded for CuABpy at two concentrations 0.05 mM and 0.5 mM. The spectra are depicted in Figure 10-A, see the electronic absorption data in Table 4.

The UV-visible absorption spectrum for CuABpy at the concentration of 0.5 mM is compared with the UV-visible absorption spectrum for the precursor, CuA, and the mixture of 0.5 mM CuA with 2 eq Bpy, as depicted in Figure 10-B. The electronic absorption data are listed in Table 8. Compared the spectra of the adduct CuABpy with those of the mixtures of CuA and Bpy, it is clear that the adduct has been formed in these mixture and its higher amount is presented in the mixture of 0.5 mM CuA with 2 eq of Bpy.

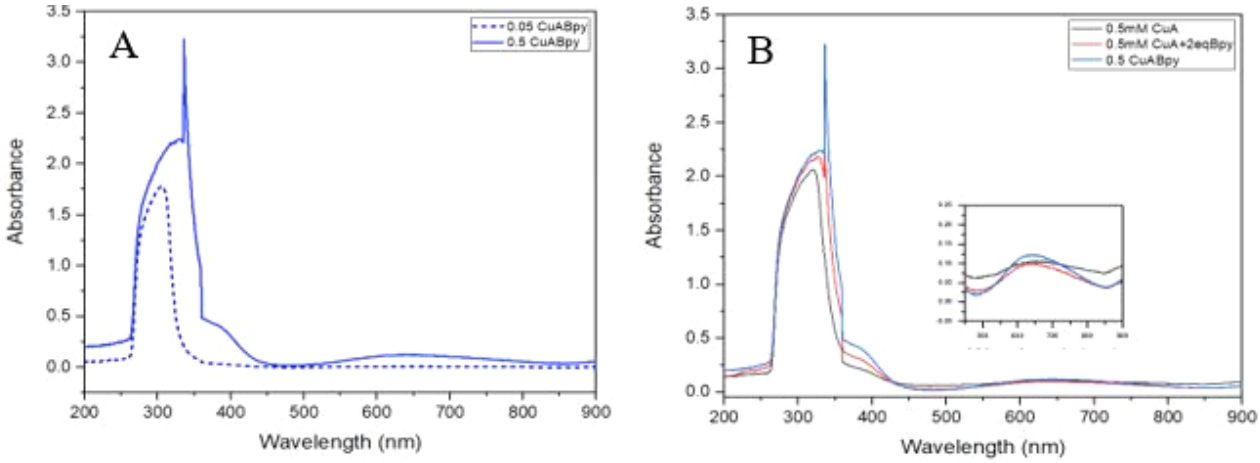

Figure 10: UV-visible absorption spectra of (A) 0.05 mM (dotted line) and 0.5 mM (solid line) of CuABpy complex (B) 0.5 mM CuA (black line), mixture of 0.5 mM CuA with 2eq Bpy (red line), and 0.5 mM of CuABpy complex in DMF at r.t by using quartz cell with path length of 1 cm

Table 8: The electronic absorption data of 0.5mM and 1mM of $V_2^{2+}.2PF_6$, CuA and CuA-Cl complexes and their mixture with 1 and 2 equivalent of $V_2^{2+}.2PF_6^-$, 0.5mM, and 1mM of $V_2^{2+}.2PF_6$, CuA, and CuA-Cl complexes and their mixture reduced by activated zinc powder at DMF

Complex	λ_{max}/nm ($\varepsilon/M^{-1}.cm^{-1}$)
0.5mM CuA +1eq $V_2^{2+}.2PF_6^-$+24 hour	316 (4130), 359 (490), 625 (60)
0.5mM CuA +1eq $V_2^{2+}.2PF_6^-$+ Zn	328 (2310), 359 (990), 384 (770), 608 (310)
0.5mM CuA +2eq $V_2^{2+}.2PF_6^-$+24 hour	324 (4310), 336 (3690), 359 (1048) 621 (120)
0.5mM CuA +2eq $V_2^{2+}.2PF_6^-$+ Zn	327 (4310), 358 (3690), 382 (1048), 392 (480), 590 (288)
0.5mM CuA-Cl+1eq $V_2^{2+}.2PF_6^-$+24 hour	306 (2160), 359 (410), 444 (160), 850 (30)
0.5mM CuA-Cl+1eq $V_2^{2+}.2PF_6^-$+Zn	281 (3050), 359 (650), 592 (460)-900 (270)
0.5mM CuA-Cl+2eq $V_2^{2+}.2PF_6^-$+24 hour	316 (4090), 359 (460), 816 (40)
0.5mM CuA-Cl+2eq $V_2^{2+}.2PF_6^-$+Zn	326 (4770), 359 (2300), 382 (1540), 611 (290)

The UV-Visible spectra of both CuA-Cl complex (the black line) and its mixture with 1eq (the blue line) and 2eq (the red line) of 4,4`-Bipyridine are recorded in DMF media at two concentrations of CuA-Cl: low at 0.05 mM and high at 0.5 mM as shown in Figures 11 (A and B) and 14 (A and B), respectively. The electronic absorption data are listed in Table 4.

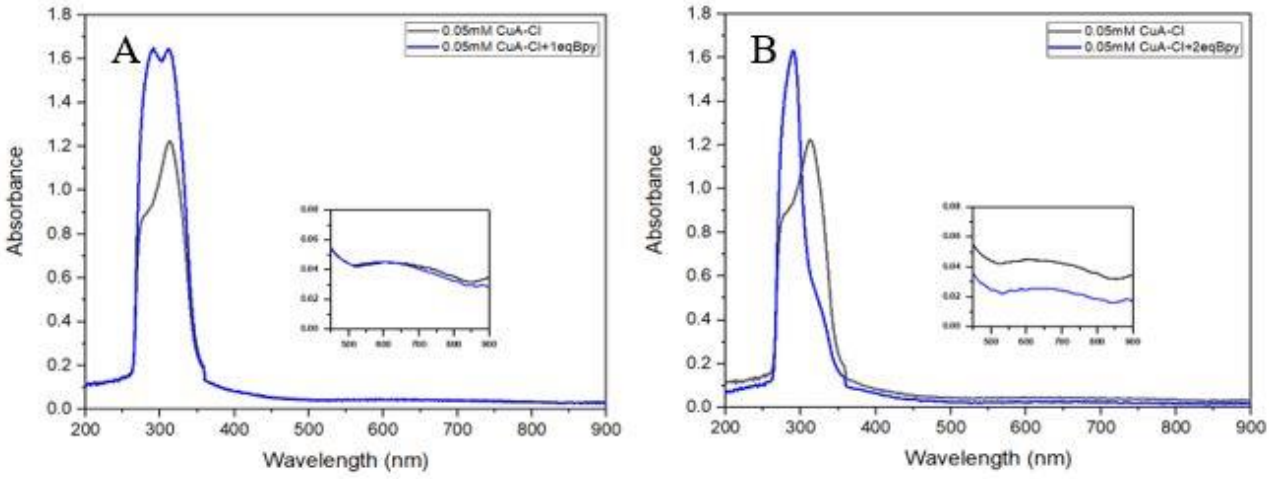

Figure 11: UV-Visible absorption spectra of 0.05 mM CuA (black lines in A and B), 0.05 mM CuA with 1eq Bpy (blue line in A), and 0.05 mM CuA with 2eq Bpy (blue line in B) in DMF at r.t by using quartz cell with path length of 1 cm

At low concentrations of CuA-Cl and Bpy mixtures, the d-d transitions of CuA-Cl occurred at 605 nm is shifted to 608 nm (red shifts) and 619 nm (red shifts) for CuA-Cl mixtures with 1 eq and 2 eq Bpy, respectively. It seems that the differences in the d-d transitions noted for CuA-Cl and 2 eq of Bpy are more obvious than those of CuA-Cl and 1 eq Bpy compared with d-d transitions of free CuA-Cl. Besides, a new band appeared at 882 nm and 884 nm for CuA-Cl mixtures with 1 eq and 2 eq Bpy, respectively. The appearance of a new band and the differences in d-d transitions in mixture solutions could be correlated to the interaction happened between Cu (II) ion and Bpy and the formation of adduct compound CuA-ClBpy at the 2 eq Bpy.

At high concentrations of CuA-Cl and Bpy mixtures, the d-d transitions of CuA-Cl occurred at 725 nm is shifted to 630 nm (blue shift) and 628 nm (blue shift) for CuA-Cl mixtures with 1 eq and 2 eq Bpy, respectively. It seems that the differences in the d-d transitions noted for CuA-Cl and 2 eq of Bpy are as same as those of CuA-Cl and 1 eq Bpy compared with d-d transitions of free CuA-Cl. These differences in d-d transitions of mixtures of CuA-Cl and Bpy could be due to the complexation of Cu (II) ion to Bpy to afford the adduct compound CuA-ClBpy.

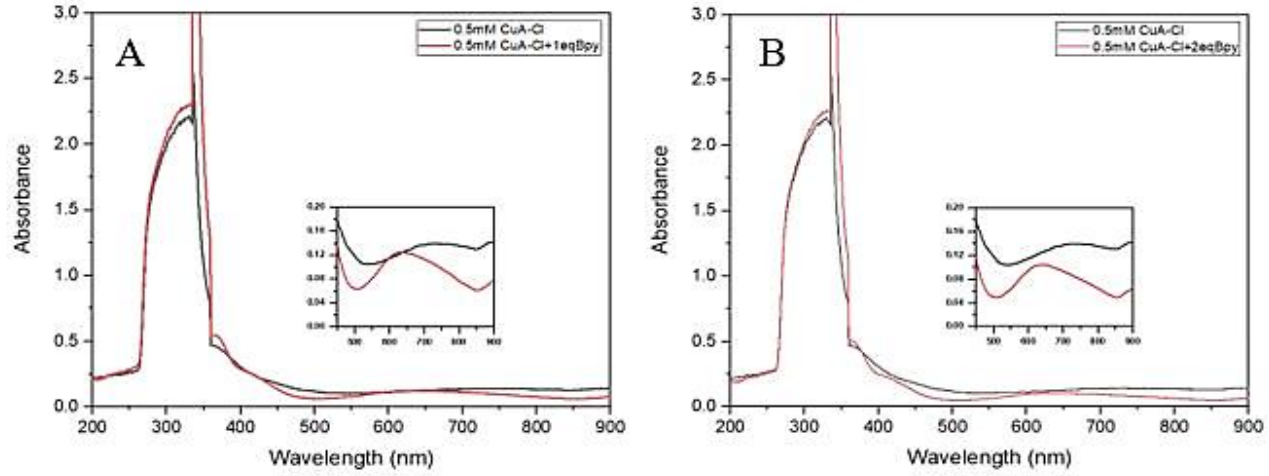

Figure 12: UV-Visible absorption spectra of 0.5 mM CuA (black lines in A and B), 0.5 mM CuA with 1eq Bpy (red line in A), and 0.5 mM CuA with 2eq Bpy (red line in B) in DMF at r.t by using quartz cell with path length of 1 cm

The complex, CuA-Cl is dissolved in the minimum amount of acetonitrile and mixed with big amount of 4,4`-bipyridine which is 10 eq. It was obtained directly the adduct, CuA-ClBpy as a green precipitate, as described in the item 3.3.2. and 3.4.1.2. It was noted that the solubility and the

color of the adduct were different from that of the precursor, CuA-Cl complex. The UV-visible absorption spectra are recorded for CuA-ClBpy at two concentrations 0.05 mM and 0.5 mM. The spectra are depicted in Figure 13-A, see the electronic absorption data in Table 4.

The UV-visible absorption spectrum for CuABpy at the concentration of 0.05 mM is compared with the UV-visible absorption spectrum for the precursor, CuA, and the mixture of 0.05 mM CuA with 1 eq Bpy, as demonstrated in Figure 13-B. The electronic absorption data are depicted in Table 4. Compared the spectra of the adduct CuABpy with those of the mixtures of CuA and Bpy, it is clear that the adduct has been formed in these mixture and its higher amount is present in the mixture of 0.05 mM CuA with 1 eq of Bpy [14, 35].

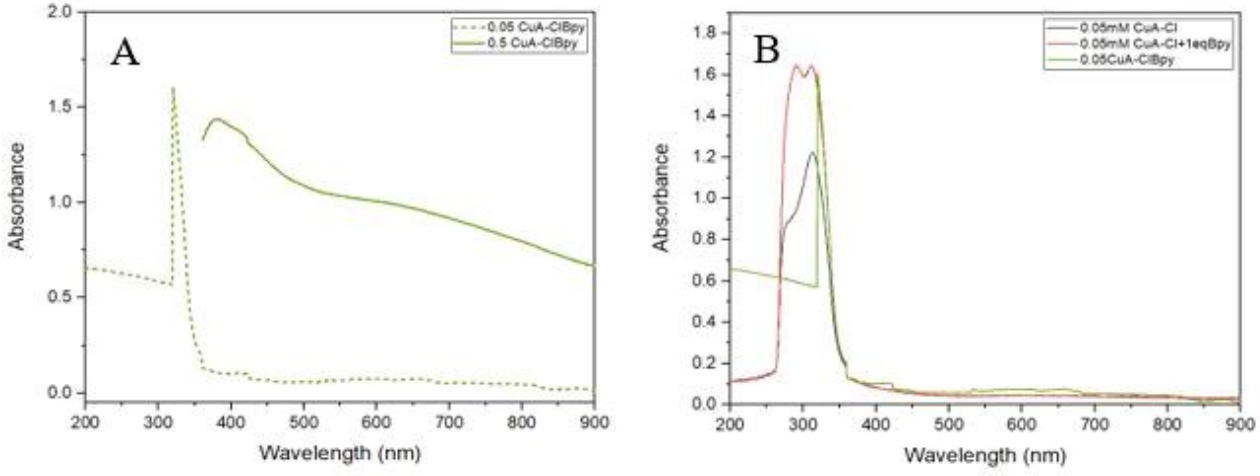

Figure 13: UV-visible absorption spectra of (A) 0.05 mM (dotted line) and 0.5 mM (solid line) of CuA-ClBpy complex (B) 0.5 mM CuA-Cl (black line), mixture of 0.5 mM CuA-Cl with 2eq Bpy (red line), and 0.5 mM of CuA-ClBpy complex in DMF at r.t by using quartz cell with path length of 1 cm

Interaction of CuA and CuA-Cl as acceptors and bisviologen, $V_2^{2+}.2PF_6^-$ as donor

The interaction between the acceptors: CuA and CuA-Cl with donor, $V_2^{2+}.2PF_6^-$ was studied in solution by UV-Visible spectroscopy. The dissolved adducts was attained by mixing 1 and 2 equivalent of $V_2^{2+}.2PF_6^-$ with high concentrations of CuA and CuA-Cl complexes, 0.5 mM.

The mixtures of 0.5 mM CuA with 1 and 2 eq $V_2^{2+}.2PF_6^-$ are recorded by using 1 eq and 2 eq $V_2^{2+}.2PF_6^-$ as blanks, respectively. This step is done to eliminate the spectrum of $V_2^{2+}.2PF_6^-$ from the spectrum of the mixture of $V_2^{2+}.2PF_6^-$ and CuA. These spectra are shown in Figures 14 and 15. The electronic absorption data are listed in Table 5.

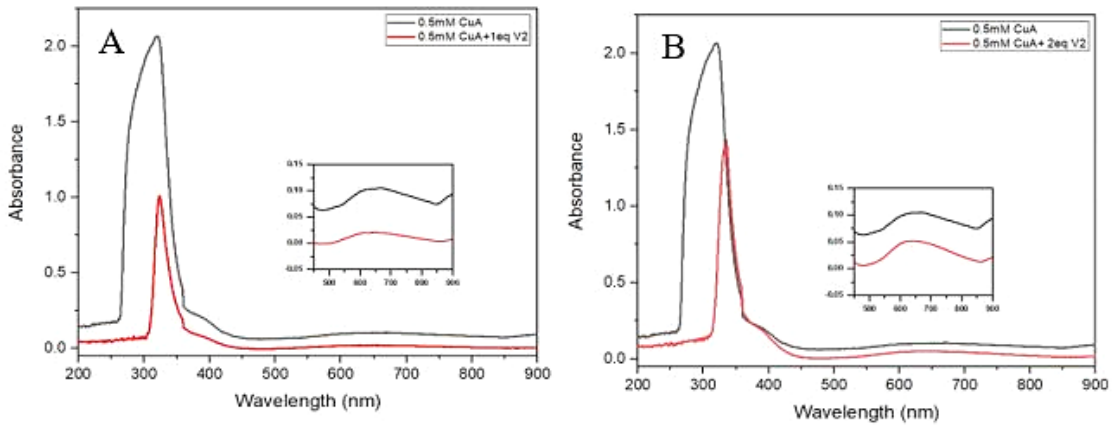

Figure 14: UV-Visible absorption spectra of 0.5 mM CuA (black lines in A and B), mixture of 0.5 mM CuA with 1eq $V_2^{2+}.2PF_6^-$ (red line in A), and mixture of 0.5 mM CuA with 2eq $V_2^{2+}.2PF_6^-$ (red line in B) in DMF at r.t by using quartz cell with path length of 1 cm. Blank for mixtures = DMF+ $V_2^{2+}.2PF_6^-$

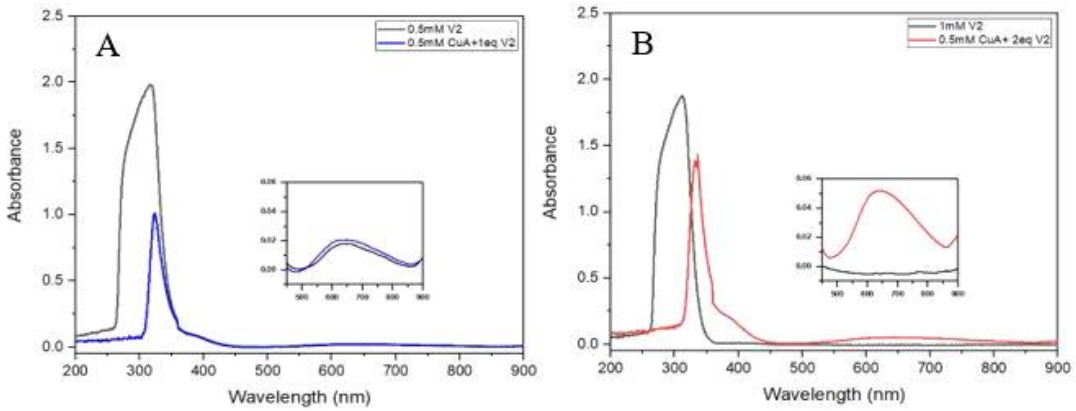

Figure 15: UV-Visible absorption spectra of 0.5 mM and 1 mM $V_2^{2+}.2PF_6^-$: black lines in A and B, respectively, mixture of 0.5 mM CuA with 1eq $V_2^{2+}.2PF_6^-$ (blue line in A), and mixture of 0.5 mM CuA with 2eq $V_2^{2+}.2PF_6^-$ (red line in B) in DMF at r.t by using quartz cell with path length of 1 cm. Blank for mixtures = DMF+ $V_2^{2+}.2PF_6^-$

After stirring of the mixtures for 10 minutes, the UV-Visible absorption spectra are recorded. The d-d transition of CuA at 671 nm is shifted to 634 nm (blue shift) for mixture of 0.5 mM CuA with 1 eq $V_2^{2+}.2PF_6^-$ and 644 nm (blue shift) for mixture of 0.5 mM CuA with 2 eq $V_2^{2+}.2PF_6^-$. The UV-Visible absorption spectra are recorded again for the same mixtures after 24 hours to follow if the interactions among CuA and $V_2^{2+}.2PF_6^-$ have been increased or not. These spectra are indicated in Figures 16 and 17. The electronic absorption data are listed in Table 5.

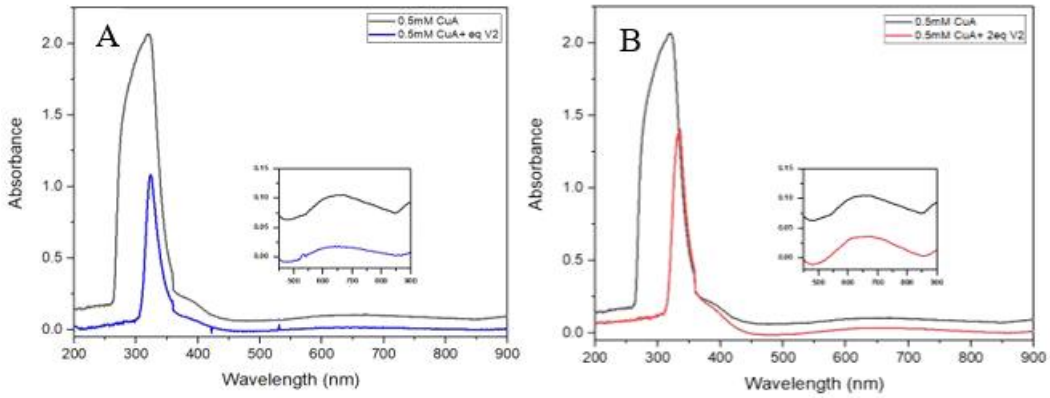

Figure 16: UV-Visible absorption spectra of 0.5 mM and 1 mM $V_2^{2+}.2PF_6^-$ (black lines in A and B) respectively, mixture of 0.5 mM CuA with 1eq $V_2^{2+}.2PF_6^-$ (blue line in A), and mixture of 0.5 mM CuA with 2eq $V_2^{2+}.2PF_6^-$ (red line in B) in DMF after 24 hours at r.t using quartz cell with path length of 1 cm. Blank = DMF+ $V_2^{2+}.2PF_6^-$

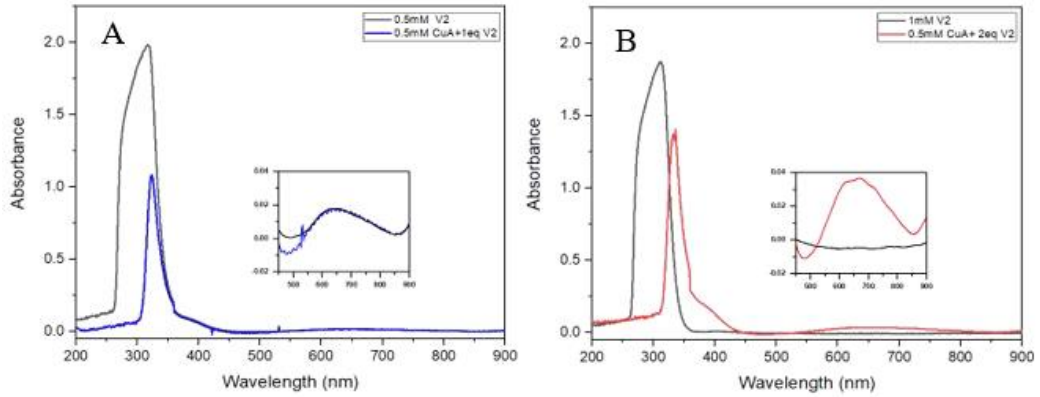

Figure 17: UV-Visible absorption spectra of 0.5 mM and 1 mM $V_2^{2+}.2PF_6^-$: black lines in A and B respectively, mixture of 0.5 mM CuA with 1eq $V_2^{2+}.2PF_6^-$ (blue line in A), and mixture of 0.5 mM CuA with 2eq $V_2^{2+}.2PF_6^-$ (red line in B) in DMF after 24 hours at r.t by using quartz cell with path length of 1 cm. Blank for mixtures= DMF+ $V_2^{2+}.2PF_6^-$

It was noted that the d-d transition of mixture of CuA with 1 eq $V_2^{2+}.2PF_6^-$ after 24 hours is shifted from 634 nm (after 10 minutes stirring) to 639 nm (red shift) for the same mixture. Also, the d-d transition of mixture of CuA with 2 eq $V_2^{2+}.2PF_6^-$ after 24 hours is shifted from 644 nm to 671 nm (red shift) for the same mixture. It seems that the differences in the d-d transitions noted for CuA with 2 eq of $V_2^{2+}.2PF_6^-$ are more obvious than those of CuA with 1 eq $V_2^{2+}.2PF_6^-$. The bigger differences in d-d transitions could be correlated to the increase of interaction between Cu (II) ion and $V_2^{2+}.2PF_6^-$ to afford the adduct solution.

The mixtures of 0.5 mM CuA-Cl with 1 and 2 eq $V_2^{2+}.2PF_6^-$ are recorded at using 1 eq and 2 eq $V_2^{2+}.2PF_6^-$ as blanks, respectively. This step is done to eliminate the spectrum of $V_2^{2+}.2PF_6^-$ from the spectrum of the mixture of $V_2^{2+}.2PF_6^-$ and CuA-Cl. These spectra are shown in Figures 18 and 19. The electronic absorption data are listed in Table 6.

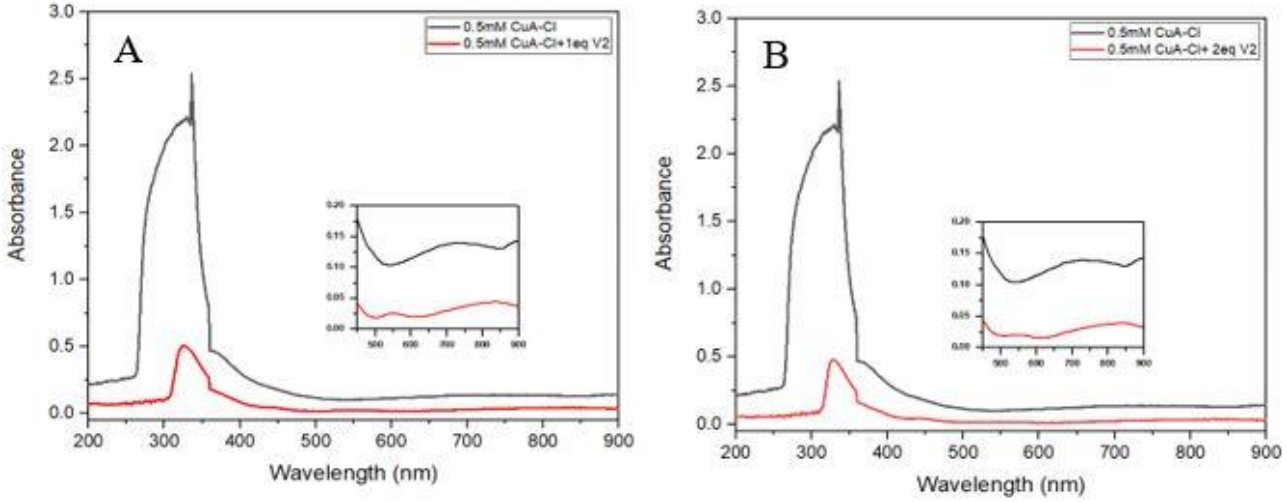

Figure 18: UV-Visible absorption spectra of 0.5 mM CuA-Cl (black lines in A and B), mixtures of 0.5 mM CuA-Cl with 1eq $V_2^{2+}.2PF_6^-$ (red line in A), and mixtures of 0.5 mM CuA-Cl with 2eq $V_2^{2+}.2PF_6^-$ (red line in B) in DMF at r.t by using quartz cell with path length of 1 cm. Blank for mixtures = DMF+ $V_2^{2+}.2PF_6^-$

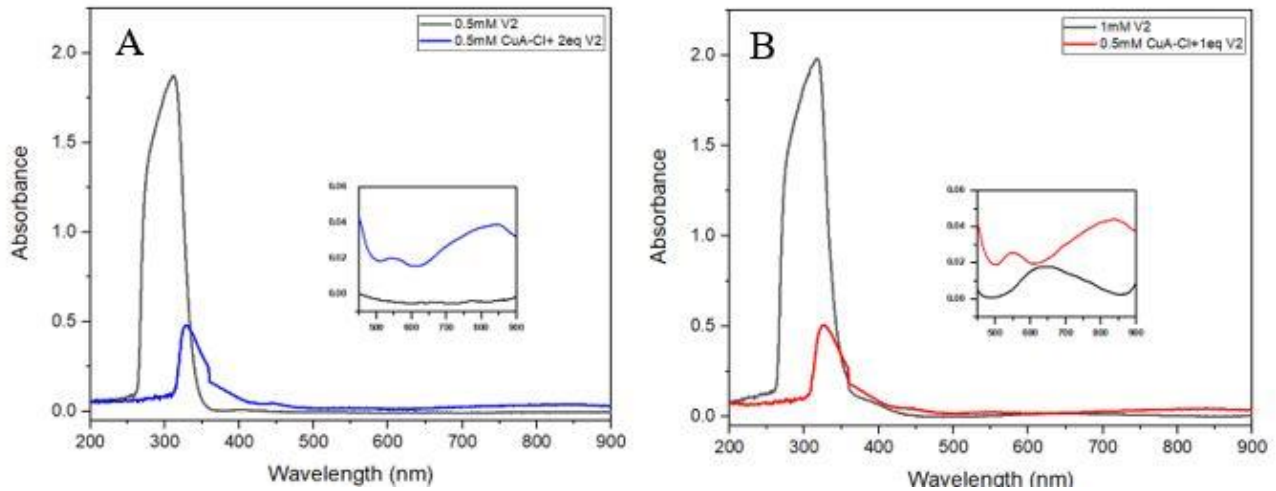

Figure 19: UV-Visible absorption spectra of 0.5 mM and 1 mM $V_2^{2+}.2PF_6^-$ (black lines in A and B) respectively, mixture of 0.5 mM CuA-Cl with 1eq $V_2^{2+}.2PF_6^-$ (blue line in A), and mixture of 0.5 mM CuA-Cl with 2eq $V_2^{2+}.2PF_6^-$ (red line in B) in DMF at r.t by using quartz cell with path length of 1 cm. Blank for mixtures= DMF+ $V_2^{2+}.2PF_6^-$

The d-d transitions of CuA-Cl occurred at 712 nm is shifted to 838 nm (red shifts) and 844 nm (red shift) for CuA-Cl mixtures with 1 eq and 2 eq $V_2^{2+}.2PF_6^-$, respectively. Besides, a new band at 445 nm, 549 appeared for CuA-Cl mixtures with 1 eq $V_2^{2+}.2PF_6^-$ as well as 445nm and 545 nm for CuA-Cl mixtures with 2 eq $V_2^{2+}.2PF_6^-$ [36, 37].

Table 6: The electronic absorption data of 0.5 mM and 1mM of $V_2^{2+}.2PF_6^-$, CuA and CuA-Cl complexes and their mixture with 1 and 2equivalent of $V_2^{2+}.2PF_6^-$ in DMF. Blank for mixtures = DMF+$V_2^{2+}.2PF_6^-$

Complex	λ_{max}/nm ($\varepsilon/M^{-1}.cm^{-1}$)
0.5mM CuA	321 (4130), 359 (770), 671 (200)
0.5mM $V_2^{2+}.2PF_6^-$	317 (3960), 359 (410), 652 (30)
1mM $V_2^{2+}.2PF_6^-$	312 (3750)
0.5mM CuA+1eq $V_2^{2+}.2PF_6^-$	324 (2022), 359 (380), 634 (40)
0.5mM CuA +1eq $V_2^{2+}.2PF_6^-$+24 hour	323 (2160), 359 (410), 385 (160), 639 (30)
0.5mM CuA+2eq $V_2^{2+}.2PF_6^-$	332 (2770), 336 (2860), 359 (900), 644 (100)
0.5mM CuA +2eq $V_2^{2+}.2PF_6^-$+24 hour	323 (2740), 336 (2810), 359 (860), 385 (360), 671 (70)
0.5mM CuA-Cl	330 (4430), 336 (5070), 358 (1620), 372 (900), 712 (270)
0.5mM CuA-Cl+1eq $V_2^{2+}.2PF_6^-$	326 (1010), 359 (530), 445 (90), 549 (50), 838 (80)
0.5mM CuA-Cl+2eq $V_2^{2+}.2PF_6^-$	328 (60), 359 (490), 445 (90), 545 (30), 844 (70)

Reduction of mixtures of CuA and CuA-Cl with bisviologen, $V_2^{2+}.2PF_6^-$

The UV-Visible absorption spectra are recorded after performing the reduction process for the previous mixtures, 0.5 mM CuA with 1 eq $V_2^{2+}.2PF_6^-$, and 0.5 mM CuA with 2 eq $V_2^{2+}.2PF_6^-$ by activated zinc powder under argon atmosphere. Also, the spectra are recorded for 0.5 mM $V_2^{2+}.2PF_6^-$ and 1 mM $V_2^{2+}.2PF_6^-$ solutions that have reduced by activated zinc powder. These spectra are shown in Figure 20. The electronic absorption data are reported in Table 7.

Table 7: The electronic absorption data of CuA and CuA-Cl complexes and their mixtures with 4,4`-Bipyridine along with those of the adducts CuABpy and CuA-ClBpy

Complex	λ_{max}/nm ($\varepsilon/M^{-1}.cm^{-1}$)
0.05mM CuA	304 (34400), 359 (1560), 620 (280), 883 (120)
0.05mM CuA+1eq Bpy	300 (34940), 359 (1320), 619 (200), 882 (100)
0.05mM CuA+2eq Bpy	306 (37240), 359 (2560), 631 (300), 896 (240)
0.5mM CuA	321 (4130), 359 (770), 671 (200)
0.5mM CuA+1eq Bpy	327 (4220), 336 (3530), 359 (1190), 638 (130)
0.5mM CuA+2eq Bpy	328 (4350), 336 (4420) 359 (1400), 385 (600), 640 (190)
0.05mM CuABpy	307 (35560), 388 (770)
0.5mM CuABpy	313 (4320), 336 (6450), 358(1990) 644 (240),
0.05mM CuA-Cl	278 (17640), 313 (24480), 359 (3660), 605 (800)
0.05mM CuA-Cl +1eq Bpy	291 (32980), 312 (32880), 359 (3820), 608 (800), 882 (580)
0.05mM CuA-Cl+2eq Bpy	289 (32600), 328 (8800), 359 (2660), 619 (500), 884 (360)
0.5mM CuA-Cl	318 (4370), 336 (5070), 359 (1570), 725 (2780)
0.5mM CuA-Cl+1eq Bpy	318 (4510), 367 (1090), 420 (480), 630 (240)
0.5mM CuA-Cl+2eq Bpy	318 (4440), 359 (2250), 369 (970), 418 (420), 628 (200)
0.05mM CuA-ClBpy	321 (31580)
0.5mM CuA-ClBpy	379 (870), 635 (1960)

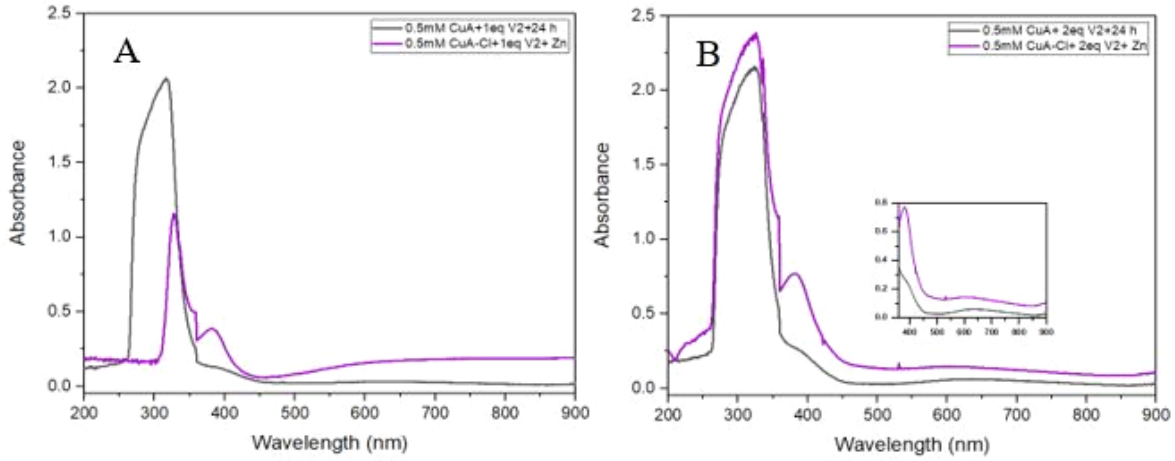

Figure 20: UV-Visible absorption spectra of mixture of 0.5 mM CuA with 1eq $V_2^{2+}.2PF_6^-$(black line in A), and mixture of 0.5 mM CuA with 2eq $V_2^{2+}.2PF_6^-$ (black line in B) after 24 hours and their reduced solutions by activated zinc powder (purple lines in A and B) in DMF at r.t by using quartz cell with path length of 1 cm

After adding activated zinc powder to the mixtures of CuA and $V_2^{2+}.2PF_6^-$ with stirring for 10 minutes under argon atmosphere, the UV-Visible absorption spectra are recorded for these mixtures. The absorption spectrum of mixture of 0.5 mM CuA with reduced 1eq $V_2^{2+}.2PF_6^-$ showed a new band at 384 nm and the d-d transition at 625 nm is blue shift to 608 nm. A wide band was appeared in the range of 608-900 nm. On the other hand, the absorption spectrum of mixture of 0.5 mM CuA with 2eq $V_2^{2+}.2PF_6^-$ showed a new band at 392 nm and a blue shift for the d-d transition from 600 nm to 590 nm. These observations are attributed to the formation of π-dimer among two viologen radicals that latter occurred after reduction by two electrons of $V_2^{2+}.2PF_6^-$ within the structure of the adducts.

The UV-Visible absorption spectra are recorded after performing the reduction process for the previous mixtures, 0.5 mM CuA-Cl with 1 eq $V_2^{2+}.2PF_6^-$, and 0.5 mM CuA-Cl with 2 eq $V_2^{2+}.2PF_6^-$ by the activated zinc powder under argon atmosphere. In addition, the spectra are recorded for 0.5 mM $V_2^{2+}.2PF_6^-$ and 1 mM $V_2^{2+}.2PF_6^-$ solutions that have been reduced by activated zinc powder. These spectra are demonstrated in Figure 21. The electronic absorption data are listed in Table 6.

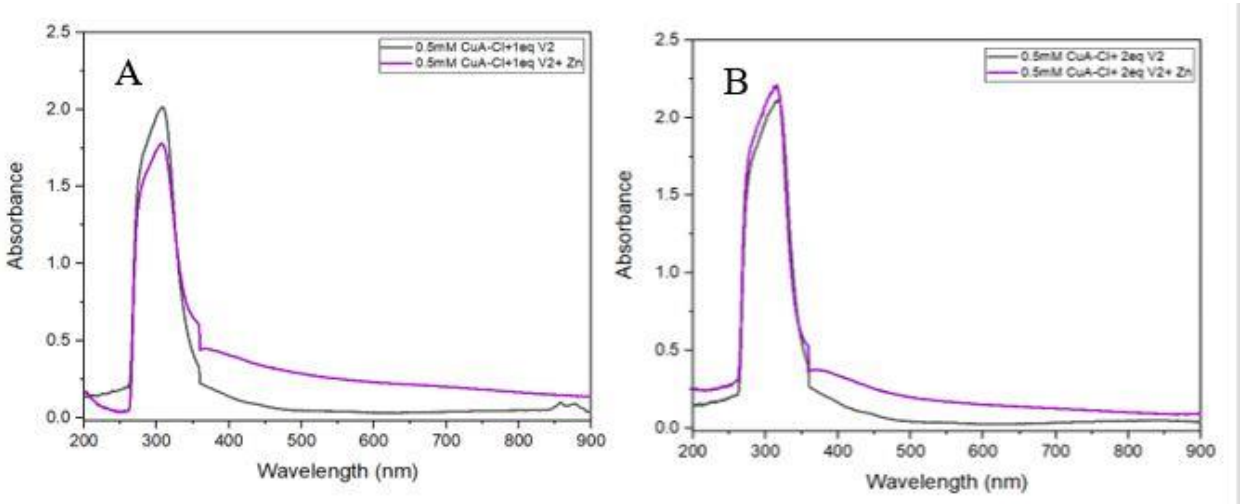

Figure 21: UV-Visible absorption spectra of mixture of 0.5 mM CuA-Cl with 1eq $V_2^{2+}.2PF_6^-$ (black line in A), and mixture of 0.5 mM CuA-Cl with 2eq $V_2^{2+}.2PF_6^-$ (black line in B) after 24 hours, and its reduced by activated zinc powder (purple line in A and B) in DMF at r.t by using quartz cell with path length of 1 cm

After adding activated zinc powder to the mixtures of CuA-Cl and $V_2^{2+}.2PF_6^-$with stirring for 10 minutes, the UV-Visible absorption spectra are recorded for these mixtures. The absorption

spectrum of mixture of 0.5 mM CuA-Cl with 1eq $V_2^{2+}.2PF_6^-$ showed a wide band in range of 592-900 nm. On the other hand, the absorption spectrum of mixture of 0.5 mM CuA-Cl with 2eq $V_2^{2+}.2PF_6^-$ revealed a new band at 382 nm and a blue shift for the d-d transition from 816 nm to 611 nm. These observations are attributed to the formation of π-dimer among two viologen radicals that latter occurred after reduction by two electrons of $V_2^{2+}.2PF_6^-$ within the structure of the adducts [38, 39].

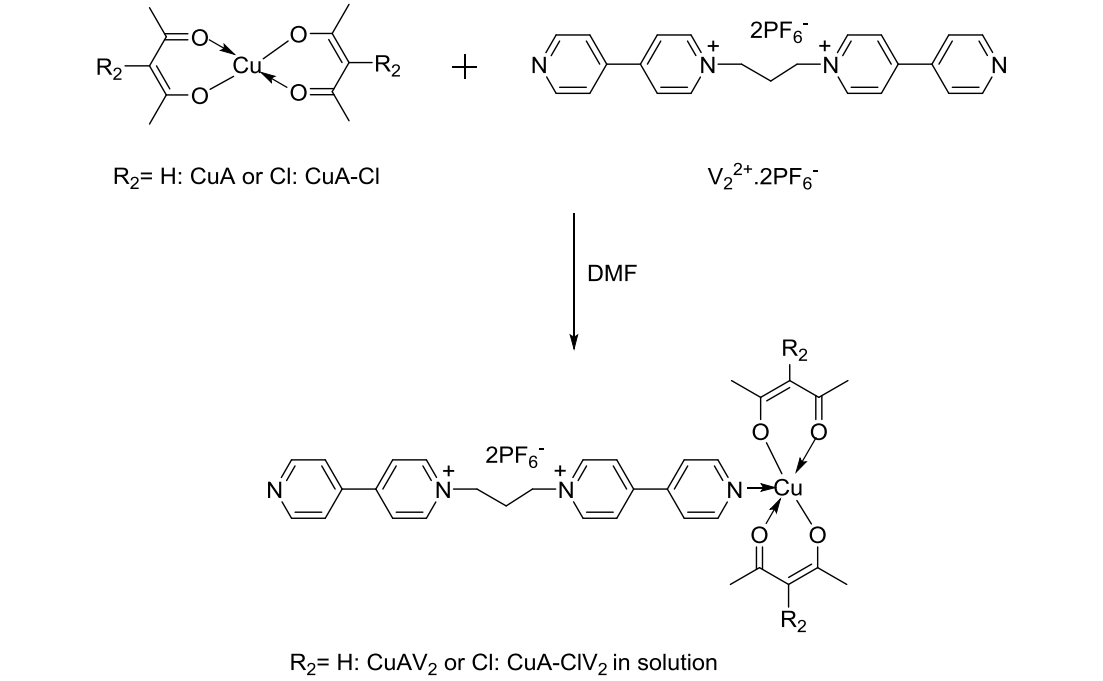

Scheme 8: reduction of $V_2^{2+}.2PF_6^-$ moieties

Conclusion

Four copper (II): CuA and CuA-Cl and their adducts CuABpy and CuA-ClBpy are synthesized and characterized them by mass, FT-IR, XRD diffraction, and UV-Visible spectrometries.

In solution, the interaction of copper (II) complexes: CuA and CuA-Cl with 4,4`-bipyridine led to the formation of the adducts: CuABpy and CuA-ClBpy. The formation of adducts in solution was studied and confirmed by the UV-Visible absorption spectroscopy. The absorption spectra of mixtures of the complexes with 4,4`-bipyridine are compared with those of both the precursor complexes and the solid adducts in DMF media.

The adducts: $CuAV_2$ and $CuA\text{-}ClV_2$ formed in DMF media are reduced by activated zinc powder and followed by absorption spectroscopy. The reduction of $V_2^{2+}.2PF_6^-$ moieties afforded the π-dimerized viologen radicals $V_2^{2\bullet}$ within the structures of the adducts: $CuAV_2$ and $CuA\text{-}ClV_2$ themselves

Funding
This research did not receive any specific grant from fundig agencies in the public, commercial, or not-for-profit sectors.

Authors' contributions
All authors contributed to data analysis, drafting, and revising of the paper and agreed to be responsible for all the aspects of this work.

Conflict of Interest
The author declared that they have no conflict of interest.

ORCID
Azhar H. Gatea
https://www.orcid.org/0000-0002-1077-7556

References
[1]. Arslan E., Lanlancette R.A., Bernal I., An historic and scientific study of the properties of metal (III) tris-acetylacetonates, *Structural chemistry*, 2017, **28**:201 [Crossref], [Google Scholar], [Publisher]
[2]. Gatea A.H., Alshamkhawy S.A., Abdul-hassan W.S., Comparison Study of Cloud Point and Solvent Extraction of Copper by 3-Chloro-2,4-pentanedione as Complexing Agent, *Journal of Medicinal and Chemical Sciences*, 2022, **5**:743 [Crossref], [Google Scholar], [Publisher]
[3]. Jassem I.A., Abdul-hassan W.S., Flafel I.A., Alshamkhawy S.A., Mahdi Z.M., Cloud Point and Solvent Extraction of Copper (II) by Bis(3-chloro acetylacetone) Ethylenediamine, *Journal of medicinal and chemical sciences*, 2022, **5**:988 [Crossref], [Google Scholar], [Publisher]
[4]. Otaghi M., Bastami M., Borji M., Tayebi A., Azami M., The effect of continuous care model on the sleep quality of hemodialysis patients. *Nephro-urology Monthly,* 2016, **8** [Crossref], [Google Scholar], [Publisher]
[5]. Mehrpour S., Najafi A., Ahmadi A., Zarei T., Pleqi V., Basiri K., Komlakh K., Abdollahi H., Emami K.H., Relationship of the optic nerve sheath diameter and repeated invasive intracranial pressure measures in traumatic brain injury patients; a diagnostic accuracy study. *Frontiers in Emergency Medicine*, 2022, **6**:e6 [Crossref], [Google Scholar], [Publisher]
[6]. Saeed M., Khalid Z., Saleem R., Synthesis and Chemical Characterization of Metals (Al, Cr, Co, Mn and VO) Complexes with Acetylacetone (β-diketone), *Journal of Natural Sciences Research*, 2017, **7**:49 [Google Scholar], [Publisher]
[7]. Darvishi A., Otaghi M., Mami S., The effectiveness of spiritual therapy on spiritual well-being, self-esteem and self-efficacy in patients on hemodialysis. *Journal of Religion and Health*, 2020, **59**:277 [Crossref], [Google Scholar], [Publisher]
[8]. Rattanapirun P., *A Study on Interactions between Some Metal Ions with Curcumin*; Price of Songkla university, 2007 [Google Scholar], [Publisher]
[9]. Kianfar A.H., Zargari S., Khanvasi H.R., Synthesis and electrochemistry of M (II) N2O2 schiff base complexes: X-Ray structure of {Ni [Bis (3-chloroacetylacetone) ethylenediimine]}, *Journal of the Iranian Chemical Society*, 2010, **7**:908 [Crossref], [Google Scholar], [Publisher]
[10]. Cook A.G., Feltman P.M., Correction to Determination of Solvent Effects on Keto− Enol Equilibria of 1, 3-Dicarbonyl Compounds Using NMR, *Journal of chemical education*, 2010, **84**:1827 [Crossref], [Google Scholar], [Publisher]
[11]. Young S.C., Smith K.T., DeBlasio J.W., Hamann C.S., Utilizing NMR to Study Structure and Equilibrium in the Organic Chemistry Laboratory. In *NMR Spectroscopy in the Undergraduate Curriculum: First Year and Organic Chemistry Courses Volume 2* (pp. 119-136). American Chemical Society. 2016 [Crossref], [Google Scholar], [Publisher]
[12]. Belova N.V., Oberhammer H., Trang N.H., Girichev G.V., Tautomeric properties and gas-phase structure of acetylacetone, *The journal of organic chemistry*, 2014, **79**:5412 [Crossref], [Google Scholar], [Publisher]
[13]. Vigato P.A., Pernzzo V., Tamburini S., The evolution of β-diketone or β-diketophenol ligands and related complexes, *Coordination Chemistry Reviews*, 2009, **253**:1099 [Crossref], [Google Scholar], [Publisher]
[14]. Xue Z., Daran J.G., Champouret Y., Poli R., Ligand adducts of bis (acetylacetonato) iron (II): a 1H NMR study, *Inorganic chemistry*, 2011, **50**:11543 [Crossref], [Google Scholar], [Publisher]

[15]. Talib H.H., Alshawi J.M., Thermal stability, synthesis of new formazan complexes derived from thiophene-2-carboxaldehyde, *Eurasian Chemical Communications*, 2021, **3**:938 [Crossref], [Google Scholar], [Publisher]

[16]. Kianfar A.H., Zargari S., Synthesis, spectroscopy and electrochemical study of cobalt (III) N2O2 Schiff-base complexes., *Journal of Coordination Chemistry*, 2008, **61**:341 [Crossref], [Google Scholar], [Publisher]

[17]. Otaghi M., Azami M., Khorshidi A., Borji M., Tardeh Z., The association between metabolic syndrome and polycystic ovary syndrome: a systematic review and meta-analysis. *Diabetes & Metabolic Syndrome: Clinical Research & Reviews*, 2019, **13**:1481 [Crossref], [Google Scholar], [Publisher]

[18]. McAfee L., Infrared and Raman spectra of inorganic and coordination compounds. Part A: theory and applications in inorganic chemistry; Part B: application in coordination, organometallic, and bioinorganic chemistry, (Nakamoto, Kazuo). 2000 [Google Scholar]

[19]. Moghadam G., Ramazani A., Nasrabadi F.Z., Ahankar H., Slepokura K., Lis T., Babaheydari A.K., Single crystal X-ray structure analysis and DFT studies of 3-hydroxyl-1,7,7-trimethyl-3-[5-(4-methylphenyl)-1,3,4-oxadiazol-2-yl]bicycle [2.2.1]heptan-2-one, *Eurasian Chemistry Communications*, 2022, **4**:759 [Crossref], [Publisher]

[20]. Waseda Y., Matsubara E., Shinoda K., *X-ray diffraction crystallography: introduction, examples and solved problems*. Springer Science & Business Media, 2011 [Crossref], [Google Scholar], [Publisher]

[21]. Prabhu Y.T., Rao K.V., Kumar V.S.S., Kumari B.S., X-ray analysis by Williamson-Hall and size-strain plot methods of ZnO nanoparticles with fuel variation, *World Journal of Nano Science and Engineering*, 2014, **4**:21 [Crossref], [Google Scholar], [Publisher]

[22]. He K., Wang C., Wei L., Chen J., Method for determining crystal grain size by x-ray diffraction, *Crystal Research and Technology*., 2018, **53**:1700157 [Crossref], [Google Scholar], [Publisher]

[23]. Tarjoman A., Vasigh A., Safari S., Borji M., Pain management in neonatal intensive care units: A cross sectional study of neonatal nurses in Ilam City. *Journal of Neonatal Nursing*, 2019, **25**:136 [Crossref], [Google Scholar], [Publisher]

[24]. McMullen A., De Haan H.W., Tang J.X., Stein, D., Stiff filamentous virus translocations through solid-state nanopores. *Nature Communications*, 2014, **5**:1 [Crossref], [Google Scholar], [Publisher]

[25]. Rabiei M., Palevicius A., Monshi A., Nasiri S., Vilkauskas A., Janusas G., Comparing methods for calculating nano crystal size of natural hydroxyapatite using X-ray diffraction, *Nanomaterials*, 2020, **10**:1627 [Crossref], [Google Scholar], [Publisher]

[26]. Zamkovsky A., Maksimova E., Nauhatsky I., Size–strain line-broadening analysis of the calcite-type borates ABO3 (A= Fe, In, Ga), *Journal of Physics: Conference Series*, 2018, **1135**: 1. [Crossref], [Google Scholar], [Publisher]

[27]. Syaima H., Rahardjo S.B., Zein I.M., Synthesis and characterization of diranitidinecopper (II) sulfate Dihydrate, *In: IOP Conference Series: Materials Science and Engineering. IOP Publishing,* 2018, **349**:012025 [Crossref], [Google Scholar], [Publisher]

[28]. Rahardjo S.B., Saraswati T.E., Masykur A., Finantrena N.N.F., Syaima H., Synthesis and Characterization of Tetrakis (2-amino-3-methylpyridine) copper (II) Sulfate Tetrahydrate. *IOP Conference Series: Materials Science and Engineering*, 2018, **349**:012056 [Crossref], [Google Scholar], [Publisher]

[29]. Konstantinovi S.S., Radovanovi B.C., Cakic Z., Vasic V., Synthesis and characterization of Co (II), Ni (II), Cu (II) and Zn (II) complexes with 3-salicylidenehydrazono-2-indolinone, *Serbian Chemical Society active member*, 2003, **68**:641 [Crossref], [Google Scholar], [Publisher]

[30]. Sallam S.A., Binuclear copper (II), nickel (II) and cobalt (II) complexes with N2O2 chromophores of glycylglycine Schiff-bases of acetylacetone, benzoylacetone and thenoyltrifluoroacetone, *Transition Metal Chemistry*, 2006, **31**:46 [Crossref], [Google Scholar], [Publisher]

[31]. Zhou M., Song L., Niu F., Shu K., Chai W., A square-pyramidal copper (II) complex with strong intramolecular hydrogen bonds: diaqua (N, N′-dimethylformamide-κO) bis [2-(diphenylphosphoryl) benzoato-κO] copper (II), *Acta Crystallographica Section C: Crystal Structure Communications*., 2013, **69**:463 [Crossref], [Google Scholar], [Publisher]

[32]. Malekshah R.E., Salehi M., Kubicki M., Khaleghian A., New mononuclear copper (II) complexes from β-diketone and β-keto ester N-donor heterocyclic ligands: structure, bioactivity, and molecular simulation studies, *Journal of Coordination Chemistry*, 2018, **71**:952 [Crossref], [Google Scholar], [Publisher]

[33]. Jasim D.J., Abbas A.K., Synthesis, identification, antibacterial, medical and dying performance studies for azo-sulfamethoxazole metal complexes, *Eurasian Chemical Communications*, 2022, **4**:16 [Crossref], [Google Scholar], [Publisher]

[34]. Palke D.G., Synthesis, Physicochemical and Biological Studies of Transition Metal Complexes of DHA Schiff Bases of Aromatic Amine, *Journal of applied organometallic chemistry*,2022; **2**:81 [Crossref], [Google Scholar], [Publisher]

[35]. Li M.J., Lan T.Y., Cao X.H., Yang H.H., Shi Y., Yi C., Chen G.N., Synthesis, characterization, DNA binding, cleavage activity and cytotoxicity of copper (II) complexes, *Dalton Transactions*, *Dalton Transactions*, 2014, **43**:2789 [Crossref], [Google Scholar], [Publisher]

[36]. Abdul-hassan W.S., *Electron-responsive molecular materials and organized assemblies based on Pi-radicals as building blocks* (Doctoral dissertation, Université Grenoble Alpes), 2018 [Crossref], [Google Scholar], [Publisher]

[37]. Abdul-Hassan W.S., *Electron-responsive molecular materials and organized assemblies based on Pi-radicals as building blocks* (Doctoral dissertation, Université Grenoble Alpes). 2018 [Google Scholar], [Publisher]

[38]. Abdul-Hassan W.S., Saint-Aman E., Royal G., Kahlfuss C., Bucher C., Molécules et matériaux moléculaires redox-et photo-stimulables, *L'Actualité Chimique*, 2018, **430**:79 [Google Scholar], [Publisher]

[39]. Courtois J., Wang B., Abdul-hassan W. S., Almasy L., Yan M., Royal G., Redox-responsive colloidal particles based on coordination polymers incorporating viologen units, *Inorganic Chemistry*, 2020, **59**:6100 [Crossref], [Google Scholar], [Publisher]

HOW TO CITE THIS ARTICLE

Azhar. H. Gatea, W. S. Abdul-Hassan, S. A. Ali, Z. M. Mahdi. Ligand Adducts of Bis(acetylacetonato) Copper(II), Bis(3-chloroacetylacetonato) Copper(II) with 4,4'-bipyridine, and Propylene Spacered Bis-viologen. *J. Med. Chem. Sci.*, 2023, 6(2) 280-303

https://doi.org/10.26655/JMCHEMSCI.2023.2.10

URL: http://www.jmchemsci.com/article_155510.html